**Phosphoproteome modifications and cortical circuit dysfunction are linked to the early-stage progression of alpha-synuclein aggregation.**

Sayan Dutta[1,7], Jennifer A. Hensel*[1,7], Alicia N. Scott*[1,7], Rodrigo Mohallem[2], Leigh-Ana M. Rossitto[3], Hammad F. Khan[4,7], Teshawn Johnson[1], Christina R. Ferreira[5], Luke A. Diehl[1], Jackeline F. Marmolejo[2,8], Xu Chen[3], Krishna Jayant[4,7], Uma K. Aryal[2,7,8], Laura Volpicelli-Daley[6], Jean-Christophe Rochet**[1,7]

*Contributed equally

**Correspondence and requests for materials should be addressed to Jean-Christophe Rochet: jrochet@purdue.edu

[1]Borch Department of Medicinal Chemistry and Molecular Pharmacology, Purdue University, West Lafayette, IN, 47907, USA

[2]Department of Comparative Pathobiology, College of Veterinary Medicine, Purdue University, West Lafayette, Indiana, 47907, USA

[3]Department of Neurosciences, School of Medicine, University of California, San Diego, 92161, USA.

[4]Weldon School of Biomedical Engineering, West Lafayette, Indiana, 47907, USA

[5]Metabolite Profiling Facility, Bindley Bioscience Center, Purdue University, West Lafayette, IN 47907

[6]Center for Neurodegeneration and Experimental Therapeutics, University of Alabama at Birmingham, Birmingham, AL 35294, USA

[7]Purdue Institute for Integrative Neuroscience, Purdue University, West Lafayette, IN, 47907, USA

[8]Purdue Proteomics Facility, Bindley Bioscience Center, Purdue University, West Lafayette, Indiana, 47907, USA

**Abstract**

Cortical dysfunction is increasingly recognized as a major contributor to the non-motor symptoms associated with Parkinson's disease (PD) and other synucleinopathies. Although functional alterations in cortical circuits have been observed in preclinical PD models, the underlying molecular mechanisms are unclear. To bridge this knowledge gap, we investigated tissue-level changes in the cortices of rats and mice treated with alpha-synuclein (aSyn) seeds using a multi-omics approach. Our study revealed significant phosphoproteomic changes, but not global proteomic or lipid profiling changes, in the rat sensorimotor cortex 3 months after intra-striatal injection with aSyn preformed fibrils (PFFs). Gene ontology analysis of the phosphoproteomic data revealed that PFF administration impacted pathways related to synaptic transmission and cytoskeletal organization. Similar phosphoproteomic perturbations were observed in the sensorimotor cortex of mice injected intrastriatally or intracortically with aSyn PFFs. Functional analyses demonstrated increased neuronal firing rates and enhanced spike-spike coherence in the sensorimotor cortices of PFF-treated mice, suggesting that aSyn seeds induced cortical circuit dysfunction. Bioinformatics analysis of the altered phosphosites indicated the involvement of several kinases, including casein kinase-2 (CK2) and MAPK (ERK), both of which have been previously implicated in PD pathology. Collectively, these findings highlight the importance of phosphorylation-mediated signaling pathways in the cortical response to aSyn pathology spread in PD and related synucleinopathies, setting the stage for developing new therapeutic strategies.

## Introduction

Parkinson's disease (PD) is a neurodegenerative disorder involving a complex array of motor and nonmotor symptoms [1,2]. A key pathological feature of PD is the death of dopaminergic neurons that project from the substantia nigra pars compacta (SNpc) to the striatum, a degenerative process underlying the disease's motor symptoms [3]. PD neuropathology is also characterized by the presence in multiple brain areas of intracellular Lewy pathology enriched with fibrillar forms of the presynaptic protein, α-synuclein (aSyn) [4,5]. Lewy pathology, consisting of both Lewy bodies and Lewy neurites, is found in the brains of individuals with PD as well as other neurodegenerative diseases associated with pathological aSyn aggregation, such as dementia with Lewy bodies (DLB) [5] and multiple system atrophy (MSA) [6], collectively known as synucleinopathies. Although current therapies effectively manage PD motor symptoms for several years, their efficacy declines over time, and no effective treatments exist to address non-motor symptoms or slow disease progression. [7].

Post-mortem analyses of PD brains at various stages of the disease indicate that aSyn aggregates initially appear in the olfactory bulb and brainstem and progressively spread to the midbrain and cortex as the disease advances [8,9]. Additionally, the injection of preformed fibrils (PFFs) of recombinant aSyn in rodent striatum leads to a spread of Lewy-like pathology through anatomically connected neuronal pathways [10-12]. aSyn pathology propagation in both synucleinopathy patients and PFF-injected rodents is believed to involve the release of aggregates from affected neurons into the extracellular space. The secreted aggregates are then taken up by neighboring healthy neurons, where they promote the aggregation of endogenous cytosolic aSyn via a seeding mechanism[13]. aSyn aggregates secreted into the CSF can be detected as a readout of underlying aSyn pathology in patients' brains using seed amplification assays [14].

aSyn is involved in the regulation of synaptic vesicle release and membrane dynamics as part of its normal physiological function [15,16]. Conversely, aSyn aggregates are known to have various pathogenic effects, including mitochondrial impairment and the dysregulation of proteostasis and lipid homeostasis [17-20]. Primary hippocampal neurons treated with aSyn PFFs show evidence of altered synaptic activity and impaired functional network connectivity [21,22]. In addition, electrophysiological analyses of brain slices from PFF-treated mice have revealed that seeded aSyn aggregation impairs neurotransmission [23]. Accordingly, intracellular seeded aSyn propagation is predicted to lead to various forms of cellular dysfunction in rodent PFF models, involving either a loss of aSyn normal function as the monomeric protein is recruited into growing aggregates [23,24], or a gain of toxic function due to the accumulation of the aggregates themselves [25]. However, information is lacking regarding the functional perturbations associated with aSyn pathology propagation in the brains of PFF-injected rodents, especially during the early stages of aggregate spread that occur well before the onset of neurodegeneration.

In this study, we carried out proteomic, phosphoproteomic, and lipid profiling of cortical homogenates from rats three months after intrastriatal injection with either aSyn PFFs or control aSyn monomer. This timeframe allowed for the formation of Lewy-like aggregates in PFF-treated animals without resulting in overt neurodegeneration or behavioral deficits. Phosphoproteomic analysis revealed pronounced PFF-dependent changes, leading to the identification of multiple phosphoprotein hits involved in cellular transport and synaptic function. These phosphoproteomic perturbations were validated in a mouse aSyn PFF model, which exhibited corresponding PFF-dependent changes in neurocircuitry function. Many of the phosphoproteins up-regulated in the brains of PFF-treated rats or mice were predicted substrates of casein kinase-2 (CK2), and the phosphoproteomic data also revealed evidence of PFF-dependent MAPK (ERK) activation that was subsequently validated through immunohistochemistry. Collectively, these results provide insights into cellular perturbations that could accompany the spread of cortical aSyn pathology in the brains of individuals with PD and other synucleinopathy disorders.

## Results

### PFF-induced aSyn aggregation leads to phosphoproteomic (but not global proteomic) changes in rat sensorimotor cortex.

To identify molecular perturbations associated with the propagation of aSyn pathology, rats were injected unilaterally in the striatum with aSyn preformed fibrils (PFFs) or monomer (Figure 1A,B) using established methods [10]. Brain samples were collected 3 months post-injection and processed for histology or proteomic, phosphoproteomic, or lipid profiling. Immunohistochemical analysis revealed that aSyn PFFs, but not the control monomer, induced the formation of aggregates that stained positive for pS129-aSyn in various brain regions, including the sensorimotor cortex (Figure 1C; Supplementary Figure 1A,B). Aggregates resembling Lewy bodies or Lewy neurites were found to be distributed among all cortical layers, especially layers IV and V, based on an analysis of sections stained for N-terminal EF-hand calcium-binding protein 1 (NECAB1), a neuronal protein specifically expressed in cortical layers IV/V (Figure 1C,D).

Analysis of cortical homogenates via liquid chromatography-tandem mass spectrometry (LC-MS/MS) led to the identification of 31,772 unique peptides (label-free quantitation (LFQ) > 0 in at least one sample) derived from 2,799 unique proteins. Following rigorous selection criteria (intensity observed in >70% of the samples in at least one of the two treatment groups), 2,159 proteins met this stringent cutoff, with only 116 proteins exhibiting a p-value below the cutoff value for significance ($p<0.05$; Figure 1E). Unsupervised 2D principal component analysis (PCA) revealed two independent overlapping clusters (Figure 1F), confirming that there were no pronounced global proteomic changes attributable to cortical aSyn aggregation at the 3-month time point. Next, we conducted similar analyses of other PD-relevant brain regions including the amygdala and SN (Supplementary Figure 1C-I). Consistent with our findings from studies of the sensorimotor cortex, no significant proteomic differences were observed in these regions when comparing the PFF- and monomer-injected animals.

Based on evidence that aSyn pathology can alter kinase localization or activity [26,27], we next examined phosphoproteomic changes in sensorimotor cortex samples from rats injected with aSyn PFFs or monomer. Changes in the phosphorylation states of synaptic proteins have been implicated as key cellular mechanisms in the dynamic regulation of neuronal synapses, even in the absence of altered protein expression levels [28-30]. We detected 3,565 unique phosphopeptides (LFQ>1) from 1,509 distinct proteins. After data filtering, 2,473 phosphosites with distinct multiplicities, mapping to 1058 proteins, were detected. Of these phosphosites, 220 (i.e., 8.9%, corresponding to 161 unique proteins) exhibited significant changes in abundance (q-value<0.1) in the brains of PFF-treated rats compared to animals injected with aSyn monomer (Figure 1G). Unsupervised PCA revealed two distinct clusters, providing evidence of differences in the phosphoproteome profile between these groups (Figure 1H). These findings suggest that seeded aSyn aggregation induces cell signaling perturbations resulting in altered phosphorylation events.

Finally, given the well-documented interaction of aSyn (in both monomeric and aggregate form) with cellular membranes [15,16,19,20], as well as evidence of changes in lipid homeostasis in the brains of PD patients [31], we determined the profiles of 11 lipid classes in cortical homogenates from aSyn PFF- and monomer-treated rats. Surprisingly, the analysis of these lipids did not reveal any significant differences or noteworthy fold changes in lipid composition between the two groups (Figure 1I). Similar lipidomic analyses were performed on homogenates prepared from amygdala and SN, yielding comparable results with no significant differences between groups (data not shown).

### Gene ontology analysis reveals alterations in cellular processes involved in synaptic transmission in the brains of PFF-injected rats.

Among the 220 significantly up-or down-regulated phosphosites (i.e., with q<0.1), a 2-fold increase or decrease in intensity was observed in 172 and 9 phosphosites, respectively, in cortical homogenates prepared from rats injected with aSyn PFFs versus monomer (Figure 2A,B). A cluster heatmap of $\log_2$-transformed intensities for the 50 lowest q-value phosphosites further highlights distinct patterns of up- and-down-regulated phosphoproteins in samples obtained from PFF- versus monomer-treated animals (Figure 2C). Only a subset of phosphosites within individual phosphoproteins exhibited PFF-dependent dysregulation, suggesting that seeded aSyn aggregation alters site-specific phosphorylation rather than overall protein expression in the rat PFF model. This conclusion is also supported by the absence of any significant changes in abundance of the parent peptides in the global proteomics dataset.

Genes associated with significantly up- and down-regulated phosphosites were further examined via gene ontology (GO) enrichment analysis. 'Synaptic organization' emerged as the most enriched cellular processes term (Figure 2D, top), involving >25 genes encoding pre- and post-synaptic scaffolding proteins (e.g., Piccolo, Bassoon, Rims1, Shank1, Shank3), proteins involved in modulating synaptic vesicle pools and neurotransmitter release (e.g., Dmxl2, Sv2A), and proteins linked to the generation of action potentials (e.g., Grin2a, Grin2b). Other highly ranked cellular processes terms included 'vesicle-mediated transport in synapse', ‘dendrite development’, and 'modulation of chemical synaptic transmission,' suggesting that the observed phosphoproteomic changes reflected alterations in synaptic function associated with PFF-mediated aSyn aggregation. Examination of enriched cellular localization terms revealed 'post-synapse’ (39 genes) and 'pre-synapse’ (32 genes) as the two most enriched terms (Figure 2D, middle), with minimal overlap. Pathways related to cytoskeletal organization were also identified from our analysis of enriched ‘cellular localization’ and ‘molecular functions’ terms (Figure 2D, middle and bottom). Moreover, many phosphosites exhibiting changes in abundance in the brains of PFF-treated rats were derived from kinases or proteins associated with kinases, suggesting that PFF administration induced changes in kinase activity. Notably, the largest cluster within the ‘molecular functions’ category included 25 ontology terms related to ‘protein kinase binding’ (Figure 2D, bottom). Kinases identified by examining our list of up- or down-regulated phosphosites for peptides that mapped to a kinase included members of the CaMK and MAPK families, as well as the AMPK complex.

Western blot analysis of selected synaptic and cytoskeletal proteins confirmed that the observed phosphoproteomic changes did not reflect major alterations in protein abundance, consistent with the global proteomics results (Supplementary Figure 2). Nevertheless, we reanalyzed the global proteomic dataset using a relaxed statistical approach, where proteins with p<0.05 (despite a q-value > 0.1) were subjected to KEGG pathway analysis. The results revealed 'Parkinson’s disease' as the most significantly enriched pathway, with 3 of 8 proteins within the pathway consisting of 20S proteasomal subunits (Supplementary Figure 3A). However, biochemical assays did not show significant differences in proteasomal activity between cortical lysates from PFF- versus monomer-injected animals (Supplementary Figure 3B), consistent with the non-significant abundance changes observed with the proteasomal hits (q>0.1).

**PFF-induced phosphoproteomic changes observed in the rat sensorimotor cortex are also evident in a mouse synucleinopathy model.**

To independently validate the PFF-mediated phosphoproteomic changes observed in the rat sensorimotor cortex, we repeated the experiment using a mouse aSyn PFF model. C57BL/6 mice were unilaterally injected with aSyn PFFs (a different preparation from the one used for the rat study) or control monomer, either in the striatum or directly in the sensorimotor cortex. After a 3-month incubation period, homogenates were prepared from the sensorimotor cortex of mice in all four groups and processed for phosphoproteomic analysis (Figure 3A,B). We identified approximately 3,500 phosphosites, with a larger proportion showing a trend towards up-regulation

compared to down-regulation in cortical homogenates of mice injected with PFFs in the striatum or cortex (Figure 3C,D; Supplementary Figure 4A,B). A total of 526 or 296 sites exhibited significant changes in abundance (q-value<0.1) in the brains of mice injected with PFFs versus monomer in the striatum or cortex, respectively. As observed in the phosphoproteomic dataset derived from analyses of rat cortex, only a subset of phosphosites within individual phosphoproteins exhibited PFF-dependent dysregulation. PCA (Figure 3E,F) and clustered heatmap analysis (Supplementary Figure 4C,D) revealed a clear separation between the PFF- and monomer-treated groups, independent of the injection site, providing strong evidence of differences in the phosphoproteome profiles between PFF- and monomer-injected animals. Moreover, the phosphosite hits observed in the brains of mice injected with aSyn PFFs in the striatum or cortex were highly correlated (Supplementary Figure 5A), further suggesting that the observed changes are due to seeded aSyn aggregation, irrespective of the site of inoculation. These findings underscore the robustness of the observed differences and suggest that seeded aSyn aggregation induces cell signaling perturbations leading to altered phosphorylation events in the mouse sensorimotor cortex.

**PFF-induced aSyn aggregation leads to synaptic dysfunction and neurocircuitry perturbations in the mouse sensorimotor cortex.**

Genes associated with significantly up- and down-regulated phosphosites in cortical homogenates of PFF-treated mice (independent of injection site) were further investigated via GO enrichment analysis. Examination of enriched cellular localization terms revealed categories related to synaptic function (e.g., ‘post-synapse’, ‘pre-synapse’, ‘axon’, ‘dendrite’), cytoskeletal organization (e.g., ‘microtubule’, ‘structural constituent of cytoskeleton’), and protein kinase binding (Figure 4A). Several phosphopeptides were found to originate from the CaMK, MAPK, and AMPK families (as observed in the rat phosphoproteomics dataset), as well as the PKA family. Additionally, GO analysis of dysregulated phosphosites derived from CAMK2G, PRKAB, PRKAR, and the MAPK kinase family in our phosphoproteomic dataset revealed 'post-NMDA receptor activation events' as the primary disrupted pathway. Similar results were obtained when the GO analysis was performed on genes associated with significantly up- and down-regulated phosphosites in cortical homogenates of mice injected in either the striatum or cortex (Supplementary Figure 5B,C).

Based on these findings, we measured circuit activity as a proxy for synaptic dysfunction in the sensorimotor cortex of mice injected with aSyn PFFs or monomer. To assess whether seeded aSyn aggregation induces changes in cortical activity, we carried out silicon probe recordings in mouse primary motor cortex 3 months after PFF or monomer injection (Figure 4B). Quantification of spiking activity across the recording session revealed sparser firing of putative layer 2/3 (L2/3) pyramidal neurons compared to layer 5 (L5) neurons, independent of PFF or monomer administration (Figure 4C). In addition, we observed notable differences in firing activity across distinct layers in relation to the injection site (Figure 4D,E). Mice injected with PFFs in the striatum showed an increase in average spiking rates in L5 (but not L2/3) pyramidal neurons compared to monomer-injected animals (Figure 4D). In contrast, both L2/3 and L5 pyramidal neurons exhibited increased spiking rates in mice injected in the cortex with PFFs versus monomer (Figure 4E). Given that striatal aSyn PFF injection leads to pathology predominantly in layer 4/5, whereas PFF injection directly into the cortex induces extensive pathology across additional layers including L2/3 [32], these data suggest that the observed layer-specific differences in firing rates between intrastriatally versus intracortically injected mice reflect the different patterns of aSyn propagation-induced dysfunction across the two sets of animals. Moreover, we infer that the precise location of aSyn seeding is a key determinant of the extent of hyperexcitability induced within the primary motor cortex. Neuronal hyperexcitability was also

observed in the cortex of GCaMP6 mice over a period of 2 to 3 months after intrastriatal or intracortical PFF injection, as demonstrated through live calcium imaging [32].

Next, we examined whether the observed increase in spiking activity among individual neurons in the cortex of PFF-treated mice was coordinated within a functionally connected neural network. To address this question, we computed the coherence between the spikes of any given pair of neurons within L2/3 and L5 (Supplementary Figure 6A), yielding a frequency-resolved measure of spike coupling across these pairs. The spike-spike coherence was markedly increased across frequencies of 5 to 20 Hz in mouse cortex 3 months after intrastriatal or intracortical injection with aSyn PFFs versus control monomer (Supplementary Figure 6B). Taken together, these data suggest that PFF injection leads to a dynamic network transition, characterized by increased fluctuations across slow (200 ms) to intermediate (50 ms) timescales, signifying enhanced correlation within the cortical neuronal population. Thus, aSyn pathology has a complex impact on translaminar cortical activity, affecting both firing rates and network connectivity. These changes in neurocircuitry function correlate with, and could potentially be a consequence of, the perturbations of synaptic activity suggested by the phosphoproteomic data.

Because our GO analysis revealed enriched cellular localization terms related to cytoskeletal organization (Figure 4A), we analyzed the spine density of cortical neurites in the brains of mice injected with aSyn PFFs or monomer. Our rationale for these measurements was based on two factors: (i) cytoskeletal destabilization is closely related to a loss of neurite integrity [33], and (ii) a decrease in dendritic spine density was previously observed in mouse cortex 5 months after intrastriatal aSyn PFF injection [34]. Contrary to these earlier findings, we observed no significant differences in spine density between mice injected with aSyn PFFs or monomer, regardless of the injection site (Supplementary Figure 7). This result indicates that a decrease in spine density does not occur in our mouse aSyn PFF model at the 3-month timepoint, despite evidence of phosphoproteomic perturbations leading to altered cytoskeletal organization in the brains of these animals.

**PFF-mediated phosphoproteomic changes are predicted to involve alterations in the activity of several kinases.**

To gain insight into the nature of the kinases – and, therefore, the potential signaling pathways – involved in aSyn PFF-mediated phosphoproteomic alterations, we examined phosphosites that were significantly up- or down-regulated in the brains of PFF-treated rats or mice for evidence of phosphorylation motif enrichment. The analysis was carried out separately for the sequence window of phosphosites showing significant increases or decreases in phosphorylation, as determined by comparing data obtained for PFF- versus monomer-treated animals within each cohort (intrastriatally injected rats, intrastriatally injected mice, and intracortically injected mice). The results are shown in Figure 5A, where the frequency of individual amino acids at each position in the phosphorylation site is represented by relative size in a sequence logo. Most of the identified phosphorylation sites contained a serine or threonine residue, suggesting that PFF-mediated changes in serine/threonine kinase activity play a major role in eliciting the observed phosphoproteomic changes. Many of the motifs that were up- or down-regulated in the brains of PFF-treated animals showed an enrichment of amino acids with negatively charged side chains, such as aspartate (D) or glutamate (E). This finding implies that acidophilic kinases, which have a high propensity to bind acidic residues in their target substrates through electrostatic interactions, exhibit altered activities in the brains of PFF-injected rats or mice. Additionally, we noted the presence of SpP and TpP motifs with high motif scores (i.e., high levels of enrichment). However, because such motifs tend to be overrepresented in enrichment studies, they were not considered further.

Next, we performed kinase predictions on the up- or down-regulated phosphosites within each cohort by comparing them to known consensus motifs targeted by specific kinases. Motifs

that were found to be enriched in our datasets are shown in a bar graph (Figure 5B), with each bar manually annotated with the corresponding predicted kinases based on their prediction scores. Among the down-regulated phosphosites in the brains of rats or mice injected with aSyn PFFs in the striatum, the motif xSpPxxxKS was significantly enriched. This sequence is predicted to be a common substrate for CDK5, GSK3, and p38 MAPK, suggesting that aSyn pathology leads to a decrease in the activity of these kinases. Conversely, up-regulated phosphosites in the brains of PFF-injected rats or mice were enriched with motifs predicted to be casein kinase 2 (CK2) substrates (e.g., SpDxD, SpDxE, and SpDxxxxE, all with motif scores >300). Additionally, we identified the canonical PKA sites RxxSp and RRxSp among the list of up-regulated phosphosites in the brains of mice injected intrastriatally or intracortically with PFFs. These results suggest that aSyn pathology leads to increased activity of CK2 and PKA in rodent brain.

**PFF-induced aSyn aggregation leads to neuron-specific activation of the MAPK (ERK) signaling pathway.**

As a second approach to identify altered protein kinases and signaling pathways contributing to phosphoproteomic alterations, we examined our list of significantly up- or down-regulated phosphopeptides for any kinase-derived peptides. In both the rat and mouse datasets, we identified phosphopeptides originating from the CaMK, MAPK, and PKA families, as well as the AMPK complex. In particular, we observed an enrichment of MAPK3 (ERK1) peptides phosphorylated on T202 or Y204 in the brains of mice injected with aSyn PFFs in the striatum or cortex (Figure 6A). This enrichment was indicative of increased ERK pathway activation, a signaling event associated with neuronal survival and axonal integrity. Immunohistochemical analysis of brain sections from mice injected intrastriatally with PFFs (but not monomer) revealed a pathology-associated increase in pERK1/2 levels, characterized by distinct punctate pERK1/2 structures in cortical neurons containing aSyn aggregates, 3 months post-injection (Figure 6B). Notably, we did not observe a corresponding increase in total ERK levels, suggesting that the observed differences were specific to phosphorylation dynamics rather than changes in overall protein expression (Supplementary Figure 8). Not all aggregate-containing neurons were positive for pERK, indicating that only a subset of these cells exhibit ERK pathway activation. A similar increase in pERK1/2 levels was observed via immunohistochemical analysis of cortical sections from PFF-injected rats (Supplementary Figure 9).

Further analysis revealed pERK1/2 puncta in aggregate-containing neurons in regions beyond the cortex, including the striatum, amygdala, and SNpc, in PFF-injected mice (Figure 6C). The proportion of aggregate-positive neurons that also exhibited pERK1/2 puncta varied among brain regions. At 3 months post-injection, the amygdala and SNpc exhibited a greater number of pERK1/2 puncta per neuron than the cortex or striatum (Figure 6D). These results suggest that cell type- or region-specific mechanisms contribute to ERK pathway activation in response to aggregate pathology. Time-course analysis in a cohort of mice also demonstrated the presence of pERK puncta at 1 and 6 months post-injection, suggesting that the ERK pathway is activated at multiple pathological stages (Figure 6E). The pERK puncta were highly colocalized with pS129-aSyn aggregates within neurons (Figure 6E, insets), a phenomenon also observed in PD brain samples using immunogold labeling [35], suggesting that pERK interacts directly with pathological aSyn inclusions.

Lastly, we re-analyzed our phosphoproteomic datasets to identify potential MAPK substrates with altered abundance in the brains of rats or mice injected with aSyn PFFs versus monomer. Using the PhosphoSitePlus library of known kinase substrates [36], we identified differentially phosphorylated MAPK substrates ($q<0.1$) across all three datasets, including 9 phosphosites on 7 unique proteins in intrastriatally injected rats, 23 phosphosites on 17 unique proteins in intrastriatally injected mice, and 11 phosphosites on 7 unique proteins in intracortically

injected mice. Notable MAPK substrates that showed PFF-dependent increases in phosphorylation included (i) potassium voltage-gated channel subfamily KQT member 2 (Kcnq2), a potassium channel subunit involved in regulating neuronal excitability (~4-fold increase in phosphorylation at S448, corresponding to S476 in the human ortholog, in the brains of intracortically injected mice, with similar trends observed in the brains of intrastriatally injected mice and rats) [37]; and (ii) phosphoglycerate kinase 1 (Pgk1), a glycolytic enzyme that regulates mitochondrial oxidative stress (~2.5-fold increase in phosphorylation at S203 in the brains of intrastriatally injected mice) [38-40].

## Discussion

The spread of aSyn pathology in the brains of rodents injected intrastriatally with PFFs follows a pattern determined by the anatomical connectivity of different brain regions to the striatum [11]. Of relevance to the current study, PFFs injected in the striatum are taken up by corticostriatal neurons via endocytosis in the synaptic region. Once internalized, PFFs are thought to escape from the endocytic compartment and induce the aggregation of cytosolic aSyn, which is abundant at the synaptic terminal of the recipient neuron [41]. Aggregates then spread gradually in a retrograde manner from the synapse to the cell body. This spread of aSyn pathology is cell type-specific, with excitatory neurons of layer IV/V (Figure 1C) being particularly susceptible to aggregate formation and propagation [42-44], closely mimicking the pathology observed in human PD [45].

Although cortical pathology becomes evident in rodents within 15 days of intrastriatal PFF administration [32], motor and cognitive deficits appear much later [12,43,46]. This slow disease progression and the modest initial behavioral phenotype closely mirror the early stages of synucleinopathy diseases such as PDD and DLB [47]. Accordingly, the rodent aSyn PFF model is well-suited for investigating early cortical cellular events that precede overt neurodegeneration. To this end, we carried out proteomic, phosphoproteomic, and lipid profiling analyses of brain homogenates from rats and mice injected intrastriatally or intracortically with aSyn PFFs, 3 months post-injection. Unexpectedly, the global proteomic analyses revealed only a small number of proteins with significant changes in abundance in the brains of PFF-injected animals across various brain regions, based on p-values but not q-values from FDR-corrected significance tests (Figure 1E; Supplementary Figure 1F,G). Comparing our results with data from one previous global proteomic analysis of aSyn PFF-injected mice revealed substantial overlap between our list of dysregulated proteins and those identified in the earlier study [48]. However, we did not observe statistically significant differences in the levels of these proteins between PFF- and monomer-injected animals, likely due to our study's limited power relative to the variability of the global proteomics data, or perhaps because global expression changes become more pronounced at later times post-injection. This issue with statistical power may also have contributed to the lack of significantly dysregulated lipids revealed by our lipid profiling analysis of brain homogenates (Figure 1G).

In contrast to the low hit rate observed in our global proteomic study, phosphoproteomic analysis led to the identification of 220 phosphosites from 161 proteins that were differentially regulated in cortical homogenates of PFF- versus monomer-injected rats, with most being up-regulated ≥ 2-fold (Figure 2A). Similar results were obtained with mice injected with aSyn PFFs in the striatum or cortex (Figure 3; Supplementary Figure 4). Among the differentially phosphorylated proteins observed in PFF-treated rats or mice were pre- and post-synaptic scaffolding proteins, proteins involved in synaptic vesicle pool regulation and release, and proteins involved in postsynaptic signaling. GO analysis of the proteins associated with the top differentially regulated phosphosites further validated disruptions of synaptic function in the brains of PFF- versus monomer-injected animals (Figures 2D, 4A; Supplementary Figure 5B,C). Changes in cellular pathways involved in synaptic function have also been observed in global transcriptomics analysis of brain samples from aSyn PFF-injected mice and PD patients [44,49,50]. However, in contrast to these studies, we failed to observe changes in total synaptic protein expression levels in rats (Supplementary Figure 2). This discrepancy may reflect a divergence between mRNA and protein expression changes, as reported by others [51,52].

Previous studies have demonstrated that acute synaptic depolarization significantly alters the synaptic phosphoproteome [29,30]. Here, we show that chronic protein aggregation similarly disrupts the phosphorylation states of synaptic proteins. However, we observed minimal overlap between the phosphosites altered in our study and those reported from earlier analyses of acute depolarization. In addition, the serine phosphorylation sites identified here were not significantly

enriched for the RxxS motif, a known CaMKII target during $Ca^{2+}$ influx [29,30]. Together, these results suggest that the phosphoproteomic changes observed in the brains of PFF-treated rats or mice are likely driven by chronic, PFF-induced signaling disruptions rather than acute $Ca^{2+}$ influx. These findings are consistent with previous reports of aberrant synaptic connectivity in brain samples from PD or DLB patients, as well as in rodent synucleinopathy models, where the degree of synaptic dysregulation is associated with aggregate burden [22,23,49]. aSyn is known to localize to the synaptic terminal, where it interacts with other synaptic proteins and plays a key role in synaptic vesicle homeostasis [41,53,54]. We propose that the recruitment of monomeric aSyn into aggregates displaces it from its normal synaptic location[23,24], leading to altered synaptic protein distribution, disrupted activity, and changes in synaptic phosphorylation, ultimately impairing synaptic function and causing circuit irregularities. Similar to the results presented here, phosphoproteomic analysis of cortical samples from AD patients at various stages of disease revealed changes in cellular pathways related to synaptic function [55]. This finding suggests that dysregulation of synaptic phosphoproteins in the cortex may be a common molecular feature underlying cognitive deficits associated with neurodegenerative disorders such as PD and AD.

Additional differentially regulated phosphopeptides in the brains of PFF-treated rats or mice were derived from proteins with molecular functions related to cytoskeletal homeostasis (Figures 2D, 4A; Supplementary Figure 5B,C). Among the most highly phosphorylated proteins in this category were Map1a, Map1b, and Map2, key components of pre-and post-synaptic terminals [44]. PFF-mediated perturbations of these and other cytoskeletal proteins could account for previously reported decreases in axonal transport in primary neurons treated with aSyn PFFs [21]. Moreover, these perturbations could potentially contribute to decreases in spine density observed in the brains of PFF-injected mice during later disease stages (e.g., 5 months after injection), as reported by Herms and colleagues [34], although spine density was unaffected in our early-stage model (Supplementary Figure 7).

The dysregulation of synaptic and cytoskeletal phosphoproteins in PFF-injected rodents suggested that neurocircuitry function might be altered in the brains of these animals. In support of this idea, we observed lower spike rates and altered spike coherence in the sensorimotor cortex of mice injected with aSyn PFFs, either intrastriatally or intracortically (Figure 4D,E). Additional studies by our group revealed that changes in neurocircuitry function appear as early as 4 weeks after PFF injection and are characterized by increases in the amplitude of 'beta events' (spontaneous bursts of beta transients) driven by NMDA receptor and voltage-gated $Ca^{2+}$ channel (VGCC) signaling [32]. Our phosphoproteomic data provide a molecular basis for these neurocircuitry disruptions, implicating dysregulation of NMDA receptor-related phosphoproteins such as Grin2a/2b, Shank3, and the Dlg family in PFF-injected mice (see Figures S10 and S11 in ref. [32]), as well as VGCC subunits Cacna1b and Cacnb1 in PFF-injected rats (this study). Future research will aim to determine whether the observed phosphoproteomic changes affecting synaptic proteins, cytoskeletal components, NMDA receptors, or VGCCs contribute directly to the neurocircuitry alterations evident in the brains of seed-injected rodents.

Examination of the up- or down-regulated phosphosites for enriched consensus motifs targeted by specific kinases revealed decreased CDK5, GSK3, and p38 MAPK activities, as well as increased CK2 and PKA activities, in the brains of PFF-injected rats or mice (Figure 5). The PFF-dependent up-regulation of CK2 activity is particularly compelling given this kinase's association with PD pathology. Specifically, CK2 phosphorylates aSyn on residue S129, a hallmark modification of Lewy bodies and neurites in the brains of synucleinopathy patients [56,57]. Furthermore, the CK2 regulatory beta subunit, CK2β, has been shown to co-localize with pS129-aSyn aggregates in the SNpc [27]. As one possible mechanism, CK2β recruitment into aSyn aggregates could result in an increased concentration of free catalytic subunits, CK2α and CK2α', in the synapse, leading to dysregulated (increased) catalytic activity and altered phosphorylation of CK2 targets [58]. Alternatively, changes in CK2β phosphorylation at residues S3, S4, and S209, as observed in our phosphoproteomic dataset, could contribute to the increased CK2 activity in

the brains of PFF-injected rats or mice [59,60]. Because CK2 is highly expressed in glial cells, especially astrocytes [61], its activation in these cells could also contribute to seed-induced increases in CK2-mediated phosphorylation observed in rodent brain homogenates.

Further analysis of the significantly altered phosphopeptides revealed kinase-derived peptides from the MAPK (ERK) family, along with the CaMK and PKA families and the AMPK complex, in the brains of PFF-injected rats or mice. Activation of the ERK pathway has not been previously demonstrated in an aSyn PFF model or in other models of inducible aSyn aggregation. The evidence presented here of increased MAPK3 (ERK1) phosphorylation on residues T202 and Y204 is consistent with previous human postmortem data showing enhanced MAPK3 phosphorylation at these sites within intraneuronal granular microstructures in the cortex of DLB patients [62] and the SNpc of PD or DLB patients [63]. Our finding that puncta density per neuron varies across brain regions (Figure 6D) suggests that region-specific disease mechanisms may drive corresponding differences in Lewy body pathology [64]. Furthermore, our observation that punctate pERK structures are detectable as early as 1 month post PFF injection, well before significant neuronal loss, suggests that pERK accumulation is an early event linked to aSyn aggregation, consistent with data from a previous study of human PD brain samples [63].

Evidence that MAPK1 and other kinases such as PRKACA are associated with pS129-aSyn in Lewy bodies [63,65] implies that interactions between these kinases and pathological aSyn could play a role in the altered kinase activity driving the phosphoproteomic changes observed in the brains of PFF-treated rodents. Activation of the ERK pathway, previously linked to a loss of viability of iPSC-derived cortical neurons [66], may contribute to the cortical dysfunction observed in PFF-injected mice (Figure 4B-D). Our finding that the MAPK substrates Kcnq2 and Pgk1 exhibit increased phosphorylation in cortical homogenates from PFF-treated rodents provides insights into how enhanced MAPK activity could modulate neuronal health and function in the brains of these animals. Notably, MAPK-mediated phosphorylation of Kcnq2 on residue S448, a modification that shifts the voltage sensitivity of Kcnq2/3 heteromultimeric channels to a more depolarized state, could reduce potassium channel activity, thereby increasing excitability and glutamate sensitivity[37]. Conversely, activated MAPK could enhance neuroprotection by phosphorylating Pgk1 at S203, inducing Pgk1 mitochondrial localization that, in turn, leads to reduced oxidative stress through the inhibition of mitochondrial pyruvate metabolism [38,39]. Lastly, our observation that 'post-NMDA receptor activation events' was the primary disrupted pathway from a GO analysis of dysregulated phosphopeptides derived from the MAPK kinase family as well as CAMK2G, PRKAB, and PRKAR suggests that these kinases could contribute to the PFF-mediated dysregulation of NMDA receptor signaling discussed earlier.

In conclusion, our findings suggest that seeded aSyn aggregation induces significant changes in protein phosphorylation, largely driven by increased CK2 activity, in the sensorimotor cortex of rats and mice injected with aSyn PFFs. In turn, these phosphoproteomic changes disrupt key signaling pathways linked to NMDA receptor function, VGCC activity, and cytoskeletal dynamics and are accompanied by neurocircuitry dysfunction. The involvement of additional kinases with altered activity, including PKA, CDK5, GSK3, and p38 MAPK, underscores the complex interplay of signaling pathways contributing to aSyn-mediated neuronal dysfunction. Our findings underscore the value of phosphoproteomics in capturing molecular phenomena such as ERK pathway activation, a key pathological biomarker in synucleinopathy progression that has been challenging to detect using other omics approaches, while highlighting the relevance of the aSyn PFF model in recapitulating early pathological changes. Understanding the molecular mechanisms linking aSyn-induced phosphoproteomic changes to neurocircuitry impairment will be critical for developing therapies to mitigate cognitive decline in PD and other synucleinopathy disorders.

## Experimental Methods

### Recombinant aSyn protein purification

Mouse recombinant aSyn was purified as described [67,68]. *E. coli* BL21 (DE3) cells transformed with the bacterial expression vector pT7-7 encoding mouse aSyn were incubated in LB medium supplemented with ampicillin (100 µg/mL) at 37°C until the optical density at 600 nm reached 0.5-0.6. Protein expression was induced with isopropyl β-D-1-thiogalactopyranoside at a final concentration of 1 mM, followed by incubation at 37°C for 4 h. The cells were then harvested by centrifugation, resuspended in lysis buffer (10 mM Tris HCl, pH 8.0, 1 mM EDTA, 0.25 mg/mL lysozyme), and lysed using a French press cell disruptor (Thermo Electron, Waltham, MA) at > 1000 psi. The lysate was treated with 0.1% (w/v) streptomycin sulfate to precipitate DNA and then clarified by centrifugation. The supernatant was subjected to partial purification via two successive ammonium sulfate precipitations (30% and 50% w/v saturation) at 4°C. The resulting pellet was resuspended in 10 mM Tris-HCl (pH 7.4), and the suspension was boiled at 95°C for 15 min. Following centrifugation at 13,500 × g at 4°C for 20 min to precipitate denatured proteins, aSyn was purified from the supernatant via successive fractionations using: (i) a HiLoad 16/600 Superdex 200 pg size exclusion column (Cytiva, Marlborough, MA), with elution performed in 10 mM Tris HCl (pH 7.4); and (ii) a HiPrep Q HP 16/10 or DEAE anion exchange column (Cytiva), with elution performed using a linear gradient of 25 mM to 1 M NaCl in a buffer consisting of 10 mM Tris HCl (pH 7.4) and 1 mM EDTA. Fractions enriched with aSyn or aSyn-mVenus (identified via SDS-PAGE with Coomassie blue staining) were pooled, and the solution was dialyzed against PBS (10 mM $Na_2HPO_4$, 1.8 mM $KH_2PO_4$, 2.7 mM KCl, and 137 mM NaCl, pH 7.4). aSyn preparations used for PFF formation were depleted of endotoxin using the Pierce high-capacity endotoxin removal resin (Thermo Fisher Scientific #88277, Waltham, MA) to 0.018 units/µg of protein (3). The purified protein was stored at -80°C until use, with a final purity of approximately 95%.

### Preparation of aSyn PFFs

A 500 µL solution of monomeric mouse aSyn (5 mg/mL) was filtered through a 0.22 µm filter (Corning #8160, Corning, NY) and incubated in a sterile 1.5 mL microcentrifuge tube at 37 °C for 7 days with continuous agitation at 1,000 rpm (123 x g) in a Thermomixer (BenchTop Lab Systems #BT917, St. Louis, MO). The resulting fibrils were concentrated by centrifugation at 13,000 x g for 10 min, and the pellet was resuspended in 250 µL of Dulbecco's phosphate-buffered saline (DPBS; Cytiva). An aliquot of the fibril suspension (5 µL) was incubated with 8 M guanidine hydrochloride at 22°C for 1 h to dissociate the fibrils into monomers. The aSyn concentration was determined via absorbance measurements at 280 nm using a Nanodrop spectrophotometer, with an extinction coefficient of 7450 $M^{-1}$ $cm^{-1}$. aSyn fibrils were stored at −80°C as 25 µL of aliquots at a concentration of 5 mg/mL. Prior to use, aliquots were thawed and sonicated in ethanol-sterilized sonicating tubes (Active Motif #53071, Carlsbad, CA) using a cup horn sonicator (Qsonica #q700, Newtown, CT) at 30% power (~100 W/s) with a cycle of 3 s on and 2 s off, for a total 'on' time of 15 min, while maintaining the bath temperature between 5 and 15 °C.

### Transmission electron microscopy

Recombinant aSyn fibrils were analyzed by negative stain transmission electron microscopy (TEM) as described [69,70]. Briefly, 3 µL of fibril suspension (≤ 0.5 mg/mL) was applied to a glow-discharged, carbon-coated copper TEM grid (Electron Microscopy Sciences #CF400CU, Hatfield, PA) and incubated at 22°C for 45 s. The grid was rinsed with deionized water, and 3.5 µL of 1% (w/v) phosphotungstic acid (PTA) was applied as a contrast agent. After a 1-minute incubation, excess PTA was removed by blotting with Whatman filter paper (Cytiva), and the grid was air-dried. Imaging was performed using an FEI Tecnai T12 Transmission Electron

Microscope (Thermo Fisher Scientific) operating at 80 kV. Gatan DigitalMicrograph software (Gatan Microscopy Suite, Pleasanton, CA) was used to capture the images.

**Intracranial PFF injections**

All methods for working with animals were conducted using protocols approved by the Purdue Animal Care and Use Committee (PACUC). In one set of experiments, 3- to 4-month-old male Sprague Dawley rats (Envigo, Indianapolis, IN) were secured in a stereotaxic frame (Kopf Instruments, Tujunga, CA) and anesthetized with isoflurane. A suspension of sonicated aSyn PFFs or a solution of control, monomeric protein (4 µL, 5 mg/mL) was injected into the striatum (coordinates: ± 3.5 mm lateral, 0 mm posterior to bregma; 4.5 mm ventral from dura) at a constant flow rate of 0.5 µL/min using a 10 µL Hamilton syringe (Hamilton, Reno, NV) fitted with a 30-gauge needle with a 45$^{o}$ angled tip. The needle was left in place for 5 min post-infusion to prevent backflow. In a second set of experiments, 3- to -4-month-old male C57BL/6 J mice (The Jackson Laboratory #000664, Bar Harbor, ME) underwent stereotaxic injections of aSyn PFFs or monomer (5 mg/mL) into either the primary motor cortex (1 µL delivered at ± 1.8 mm lateral, 0.3 mm anterior to bregma; 0.7 mm ventral from dura) or the striatum (1.5 µL delivered at ± 2 mm lateral, 1 mm posterior to bregma; 2.5 mm ventral from dura). Injections were performed using a 10 µL syringe fitted with a 33-gauge needle at a flow rate of 50 to 100 nL/min. Post-surgical care included administration of ketoprofen (5 mg/kg in normal saline) to rats and 5 mg/kg carprofen plus 6 mg/kg dexamethasone to mice, immediately after surgery and 48 h later.

**Brain tissue processing**

Rats or mice were euthanized by an overdose with sodium pentobarbital (50.9 mg/mL) and transcardially perfused with cold PBS. Animals designated for immunohistochemical (IHC) analysis were additionally perfused with 4% (w/v) paraformaldehyde (PFA) in PBS. Brains were quickly removed after decapitation, post-fixed overnight in the same PFA solution, and cryoprotected in 30% (w/v) sucrose in water at 4°C. Coronal sections (40 µm thick) were prepared using a frozen sliding microtome (Thermo Scientific Microm HM430). Sections were stored at -20°C in cryoprotectant solution (30% w/v sucrose and 30% v/v ethylene glycol in 0.1 M phosphate buffer, pH 7.4) until IHC analysis. For animals designated for proteomic and lipid profiling, specific brain regions (sensorimotor cortex, amygdala, and SN) were isolated immediately after perfusing with cold PBS, flash-frozen in liquid nitrogen, and stored at -80°C until further analysis.

**Immunohistochemistry**

Free-floating sections were washed 3 times for 10 min each in PBS to remove residual cryoprotectant solution and then incubated in PBS containing Triton X-100 (1% v/v) for 60 min. The sections were blocked in a solution of 10% (v/v) normal donkey serum in PBS supplemented with Triton X-100 (0.3% v/v) (PBST) for 90 min and then incubated with primary antibody solution prepared in PBST containing 1% (v/v) normal donkey serum overnight at 4°C. After washing in PBS (3 x 10 min), the sections were incubated with Alexa fluor-conjugated secondary antibodies (Jackson ImmunoResearch Laboratories, West Grove, PA; 1:500 dilution) at 22°C for 90 min. After a final round of three 10-min washes in PBS, the tissues were mounted on slides, allowed to dry overnight, and sealed with coverslips using DPX mounting media (Electron Microscopy Sciences #13512). The primary antibodies used in these experiments included antibodies specific for tyrosine hydroxylase (Millipore Sigma #AB1542, Burlington, MA; 1:1000), NECAB1 (Thermo Fisher Scientific #PA5-54849; 1:500), ERK1/ERK2 (Thermo Fisher Scientific #13-6200; 1:500), phospho-ERK1/2 (Thr202, Tyr204) (Thermo Fisher Scientific #14-9109-82; 1:500), pS129-aSyn (EP1536Y) (Abcam #ab51253, Cambridge, UK; 1:500], and pS129-aSyn (81a) (Millipore Sigma #MABN826; 1:500])**.** pERK1/2 puncta were counted, and statistical significance of differences in

puncta counts per cell body was determined using one-way ANOVA with Tukey's post hoc test (Prism software, Dotmatics, Boston, MA).

**Sample preparation for proteomic/phosphoproteomic and lipid profiling analyses**

Brain tissue samples (~15-20 mg for rat, ~10-15 mg for mouse) were resuspended in 300 µL of 25 mM ammonium bicarbonate (ABC) supplemented with protease and phosphatase inhibitors and homogenized in a Precellys Evolution tissue homogenizer using soft-tissue homogenizer CK14 tubes (Bertin Technologies SAS, Montigny-le-Bretonneux, France). The total protein concentration was measured using the bicinchoninic acid (BCA) assay (Thermo Fisher Scientific). For rat brain samples, the Bligh and Dyer (B & D) extraction method [71] was performed using lysate volumes equivalent to 25 µg of total protein. The chloroform layer was then carefully transferred to a new tube, dried in a vacuum centrifuge, and used for lipid analysis (see below). Four volumes of cold (-20°C) methanol were then added to the water-methanol layer, and samples were spun at 17,200 x g for 10 min. The supernatant was removed, and pelleted proteins were dried in a vacuum centrifuge and retained for proteomics analysis (described below). For the phosphoproteomics experiments (carried out on both rat and mouse brain samples), tissue lysate containing 500 µg of total protein was precipitated with acetone overnight. The protein pellets (for proteomics and phosphoproteomics experiments) were then resuspended in 10 µL of 8 M urea solution supplemented with 10 mM DTT and incubated at 37°C for 1 h. Next, 10 µL of alkylation reagent mixture (97.5% v/v acetonitrile (ACN), 0.5% v/v triethyl phosphine, 2% v/v iodoethanol) was added, and samples were incubated at 37°C for 1 h. After alkylation, samples were dried in a vacuum centrifuge and resuspended in 80 µL of 0.025 µg/µL trypsin (Thermo Fisher Scientific). The digestion was carried out using a barocycler (50°C, 60 cycles; 50 s at 20 kpsi and 10 s at 14.7 psi). Peptides were then desalted with a C18 silica MicroSpin column (The Nest Group, Ipswich, MA). For phosphoproteomic analysis, phosphopeptides were enriched with PolyMac spin tips (Tymora Analytical, West Lafayette, IN), following the manufacturer's recommendations.

**LC-MS/MS analysis**

Peptide analysis was performed using an UltiMate 3000 RSLC nano HPLC system (Thermo Fisher Scientific) coupled to either a Q-Exactive Orbitrap HF mass spectrometer for rat samples or an Orbitrap Fusion Lumos for mouse samples (Thermo Fisher Scientific). Both LC-MS/MS systems employed Thermo Fisher PepMap trap and analytical columns. Samples were initially loaded onto a PepMap C18 trap column (50 mm × 300 µm, 5 µm particle size, 100 Å pore size) at a flow rate of 5 µL/min for 5 minutes using buffer A (0.1% v/v formic acid in water) to desalt and concentrate peptides. Subsequent chromatographic separation was achieved using an Acclaim PepMap C18 analytical column (500 mm × 75 µm, 2 µm particle size, 100 Å pore size) operated at a flow rate of 150 nL/min. Peptides were eluted over a 160-minute gradient consisting of buffer A and buffer B (0.1% v/v formic acid in 80% v/v acetonitrile in water), as follows: 2% to 27% buffer B over 110 minutes, ramped to 40% over the next 15 minutes, increased to 100% over 10 minutes, held at 100% for 10 minutes, and finally re-equilibrated to 2% buffer B.

For both rat and mouse datasets, full MS (MS1) scans were acquired at a resolution of 60,000 (at m/z 200), followed by MS/MS (MS2) scans at a resolution of 15,000. The scan range was set to m/z 375-1600, with the RF lens set to 30%. The AGC (automatic gain control) target was set to Standard for the Lumos and $3 \times 10^6$ for the Q-Exactive HF. Maximum injection times were set to "Auto" (Lumos) or 100 milliseconds (Q-Exactive HF). Data were acquired in data-dependent acquisition (DDA) mode with a cycle time of 3 seconds and a dynamic exclusion duration of 60 seconds to reduce redundant sampling. Peptides were fragmented using higher-energy collisional dissociation (HCD) with 30% normalized collision energy and an isolation window of 1.2 m/z. All instrument parameters and workflows are consistent with previously published protocols.[32,72,73].

## Lipid profiling analysis

Brain lipids were analyzed using the MRM profiling method [74,75]. Dried lipid extracts prepared as described above were diluted in injection solvent (acetonitrile/methanol/300 mM ammonium acetate, 3:6.65:0.35 v/v) to obtain a stock solution. This solution was further diluted into injection solvent spiked with 0.1 ng/µL of EquiSPLASH LIPIDOMIX isotopically labeled lipids (Avanti Polar Lipids #330731, Alabaster, AL) for sample injection. MS data were acquired using flow-injection (i.e., without chromatographic separation) of 8 µL of the diluted lipid stock solution delivered using a micro-autosampler (G1377A) to the ESI source of an Agilent 6410 triple quadrupole mass spectrometer (Agilent Technologies, Santa Clara, CA). A capillary pump was connected to the autosampler and operated at a flow rate of 7 µL/min and a pressure of 100 bar. The Agilent 6410 was set to acquire lists of multiple reaction monitoring scans (MRMs) related to lipids. The dwell time for each MRM was 40 ms. The MRMs used were based on the Lipid Maps Standard Database (LMSD) for phosphatidylcholine (PC), phosphatidylethanolamine (PE), phosphatidylinositol (PI), phosphatidylglycerol (PG), phosphatidylserine (PS), ceramides, cholesteryl esters (CE), free fatty acids (just single ion monitoring - SIM), triacylglycerols (TAG), and diacylglycerols (DAG). The MRMs related to PC, PE, PG and ceramides were based on protonated parent ions and class-diagnostic product ions. The MRMs related to PS, PI, DAG, TAG, and CE were based on ammonium adducts for the parent ions, class-diagnostic product ions for the PS, PI, and CE lipids, and on fatty acyl neutral losses for the TAG and DAG lipids. Free fatty acids were detected as deprotonated ions in the negative ion mode. The collision energies and fragmentor and cell acceleration voltage settings were determined based on product ion scan experiments using EquiSPLASH LIPIDOMIX isotopically labeled lipids. The electrospray ionization (ESI) source parameters were gas temperature 300°C, gas flow 5.1 L/min, nebulizer 17 psi, and capillary voltage 4 kV for the positive ion mode and 3.5 kV for the negative ion mode.

## Bioinformatics analysis

Raw LC-MS/MS data were processed using the analysis platforms Maxquant (version 2.0.3.1) [76] and Perseus [77]. The data were searched against the *Rattus norvegicus* or *Mus musculus* sequence on UniProt [78] using trypsin as the proteolytic enzyme, allowing up to 2 missed cleavages. Variable modifications were specified for “methionine oxidation” and, in the case of phosphoproteomic analysis, “STY phosphorylation,” while “carbamidomethylation” was assigned as a fixed modification. Other search and data filtering parameters were set as described [79]. Raw data files were filtered based on contaminants, and intensity values were $\log_2$-transformed. Protein/peptide entries present in >70% of the samples were selected for downstream analysis. Data imputation was performed for the replacement of missing values and data quality validation. A two-sample t-test was performed (with a permutation-based false discovery rate (FDR) correction) on samples obtained from PFF- versus monomer-injected animals. Peptide sequences exhibiting a greater than 2-fold increase or decrease in abundance in the brains of animals injected with PFFs versus monomer were subsequently analyzed for gene ontology (GO) enrichment. GO analysis was performed using the Metascape bioinformatics platform (https://metascape.org) [80]. Heatmaps were generated in MATLAB, and sample clustering based on PCA was performed using the web platform MetaboAnalyst 5.0 [81].

Lipid profiling was performed as described [74,75]. The MS data were processed using an in-house script to obtain a list of MRM transitions with their respective sums of absolute ion intensities over the acquisition time. Group-average fold changes were analyzed for 11 lipid classes. To determine the group average, intensities were first filtered using a cutoff of 1.3x blank values. Fold change was plotted using Prism software. Statistical analysis was performed utilizing MetaboAnalyst 5.0. Data on relative amounts were autoscaled to obtain a normal distribution, followed by an analysis of heatmap distributions and t-tests with FDR corrections.

## Measurement of proteasomal activity

Proteasomal activity was measured in tissue lysates as described [82]. Briefly, flash-frozen tissues were lysed in 150 to 400 µL cold assay buffer (50 mM HEPES, pH 7.4, 10 mM NaCl, 1.5 mM $MgCl_2$, 1 mM EDTA, 250 mM sucrose, 1 mM freshly prepared ATP) using a 1/8-inch probe tip sonicator (Fisher Scientific, FB120 with CL-18 probe) set to 30% power, with a cycle of 1 s on and 1 s off for 30 cycles. Lysates were then spun at 13,000 × g and 4°C for 20 min, and protein concentrations in the supernatant were determined using a BCA protein assay kit. For activity measurements, proteins (15 to 30 µg) were diluted into 100 or 200 µL of assay buffer containing DTT (1 mM) and 7-amino-4-methyl coumarin (AMC) (25 µM) (Enzo Life Sciences, Farmingdale, NY). Proteasomal activity was quantified by monitoring the rate of fluorescence increase at 37°C using a Synergy fluorescence plate reader (BioTek Instruments, Winooski, VT) with excitation and emission wavelengths set to 360 nm and 480 nm. Control reactions were prepared by supplementing lysates with epoxomicin (Millipore Sigma #324800) at a final concentration of 5 µM to inhibit proteasomal activity. Statistical significance of group differences for each of the 3 enzymatic activities was assessed using one-way ANOVA (Prism software).

## Western blot analysis

Western blot analysis was performed as described [83]. Briefly, frozen brain samples were homogenized in RIPA buffer (50 mM Tris HCl, pH 7.4, 150 mM NaCl, 0.1% (w/v) SDS, 0.5% (w/v) sodium deoxycholate, 1% (v/v) Triton X-100) supplemented with protease inhibitor, and the supernatant obtained after centrifugation at 10,000 x g was mixed with Laemmli buffer (Bio-Rad Laboratories, Hercules, CA) containing 5% (v/v) β-mercaptoethanol. The samples were boiled at 95°C for 5 min, and the proteins were separated via SDS-PAGE on a 4 to 20% (w/v) polyacrylamide gradient gel (Bio-Rad) and transferred to a 0.4 µm PVDF membrane. After transfer, membranes were blocked in blocking buffer (LICORbio, Lincoln, NE) for 60 min at 22°C and then incubated overnight at 4°C with primary antibodies against synapsin (Cell Signaling Technology #D1265, Danvers, MA; 1:1000), syntaxin (Abcam #ab188583; 1:1000), synaptobrevin (Antibodies Incorporated #1933-SYB, Davis, CA; 1:1000), tau (Millipore Sigma #MAB3420; 1:500), β-actin (Millipore Sigma #A5441; 1:2000), or β-tubulin (Cell Signaling Technology #15115; 1:1000). After washing in Tris-buffered saline with Tween 20 (0.05% v/v), the membranes were incubated with secondary antibodies conjugated to infrared dyes (LICORbio) for 90 min at 22°C. Imaging was performed using a Li-Cor imaging system (Odyssey M Model 3350, LICORbio), and band intensities were quantified using the ImageJ software (NIH, Bethesda, MD). Statistical significance of band intensity differences between the 'monomer' and 'PFF' groups was determined for each protein examined on the blot using an unpaired t-test (Prism software).

## Golgi-Cox staining

Golgi-Cox staining was performed using the FD Rapid GolgiStain kit (FD Neurotechnologies, Columbia, MD). Brains were immersed in the impregnation solution and incubated for 24 h, after which they were transferred to fresh solution and stored in the dark at 22°C for 2 weeks. The brains were then placed in Solution C and incubated at 4°C for 2 d. To achieve uniform freezing, the brains were immersed in 2-methylbutane cooled to -78°C using a dry ice ethanol bath. Coronal sections (80 µm thick) were then prepared using a cryostat and mounted on gelatin-coated microscope slides. The sections were dried for 2 days, rehydrated in Milli-Q water, and treated with the developing solution. They were then dehydrated in an ethanol series (70%, 80%, and 100% v/v), cleared in xylene, and mounted using DPX mounting medium

(Electron Microscopy Sciences). Coverslips were applied to preserve the stained sections for analysis.

**Image acquisition and dendritic spine analysis**

Five dendrite sections from layer II/III pyramidal neurons in the cortical region of each mouse were identified and imaged using a laser scanning microscope (Zeiss, Oberkochen, Germany) equipped with a 60x objective lens. High-resolution images were captured from the basal compartment of each neuron and uploaded to Neurolucida 360 software (MBF Bioscience, Williston, VT). For spine density quantification, a dendritic segment of at least 10 μm in length was randomly selected from the basal compartment of each of the five neurons per mouse. Each segment was traced, and dendritic spines were manually counted using Neurolucida 360. Statistical significance of group differences in spine density was assessed using one-way ANOVA (Prism software).

**Cranial window and electrode implant**

Under sterile conditions, a custom titanium headplate was attached to the skull using vetbond and metabond dental cement. After headplate implantation, mice were allowed to recover in their home cages for 3 d. Mice underwent habituation of head fixation and running on a 6-in rotating wheel for at least one week before electrophysiological experiments were performed. On the day of the experiment, carprofen and dexamethasone were administered subcutaneously. Following previously established methods [32], a small craniotomy (< 1 mm) was made over the primary motor cortex (0.4 mm AP, 1.5 mm ML), and the dura was partially removed. A 64-channel electrode (64D Sharp, Mismanidis Lab) was inserted perpendicular to the surface of the pia using a micromanipulator (Sensapex uMp-4, Oulu, Finland). The microelectrode was positioned 1 mm into the motor cortex and allowed to settle for 20 min before recordings began. Signals were digitized at a bandwidth of 0.1 to 10 kHz and sampled at 20 kHz (Intan RHD recording system, Los Angeles, CA). Probe tracks were confirmed histologically after each experiment to verify electrode placement.

**Spike sorting**

After the recording session, the electrical signals were processed to sort action potentials from individual neurons. This sorting was accomplished using Kilosort3, followed by a meticulous manual review in Phy2. Neurons were evaluated based on waveform characteristics, stability of firing rates observed throughout the recording session, and autocorrelograms. To analyze the time-varying response of neurons, peri-stimulus time histograms were generated by creating 2000 ms windows during quiescent mouse activity. Average neural activity traces were smoothed by calculating the mean spiking activity across multiple trials and convolving by a Gaussian filter with a full-width at half-maximum (FWHM) of 10 ms. The depth at which each spike occurred was determined based on the electrode that recorded the maximum waveform amplitude. Spiking analysis was conducted on neurons exhibiting sustained activity throughout the entire recording session. Statistical significance of differences in the spiking rates of neurons in the brains of PFF- versus monomer-injected mice was determined using a ranked-sum Wilcoxon test (MATLAB).

**Analysis of spike-spike coherence**

To assess the coherence between two spiking signals, we employed discrete signal taper methods as described [84-87]. The 2000 ms trial period was segmented into multiple 400 ms intervals with a 200 ms overlap, ensuring full coverage. We removed the DC component from

each spike train and applied a single Slepian taper, resulting in an effective smoothing of 2.5 Hz for the 400 ms data windows (NW = 1, K = 1). Confidence intervals were determined using jackknife resampling, involving the exclusion of individual trials. To test whether time-locked trends in firing rate across trials influenced coherence calculations, we performed random shuffles of trial identities and recalculated coherence. This provided a baseline for coherence solely attributed to trends in firing time-locked to the trial. Further, to account for differences in firing rates across neurons within a session, a random number of neurons (5% of the total recorded units) were excluded, and the coherence was recalculated. This was done a total of 3 times to check for biasing introduced by rate-dependent spiking events. Coherence values were computed based on cross-correlations within trials, followed by cross-correlation pooling across trials and normalization by the power spectra of spike trains, which were also pooled over trials.

**Motif enrichment analysis and kinase prediction**

Logos for significantly increased or decreased phosphopeptides in binary comparisons were generated using WebLogo (version 3.7.4) [88]. Motif enrichment analysis was done using motifx (R package rmotifx version 1.0) [89]. Foreground sequences were sequences of total length 15, ± 7 amino acid residues flanking each phosphosite, that were either significantly increased or decreased in binary comparisons ($p<0.05$, $q<0.1$). Background sequences were extracted from the rat and mouse proteomes (Uniprot UP000002494 and UP000000589, respectively) using helper packages parseDB and extract Background (R package PTMphinder, version 0.1.0) [90]. The central residue was set to S, T, or Y, the minimum sequence cut-off was set to 5, and the p-value cut-off was set to $10^{-5}$. Enriched motifs are represented by their motif score, which is calculated by taking the sum of the negative log probabilities used to fix each position of the motif. Higher motif scores correspond to more specific and statistically significant motifs. Lastly, kinase prediction was performed using NetPhos3.1 online software, with positive predictions having scores >0.5 [91].

**Figure 1**

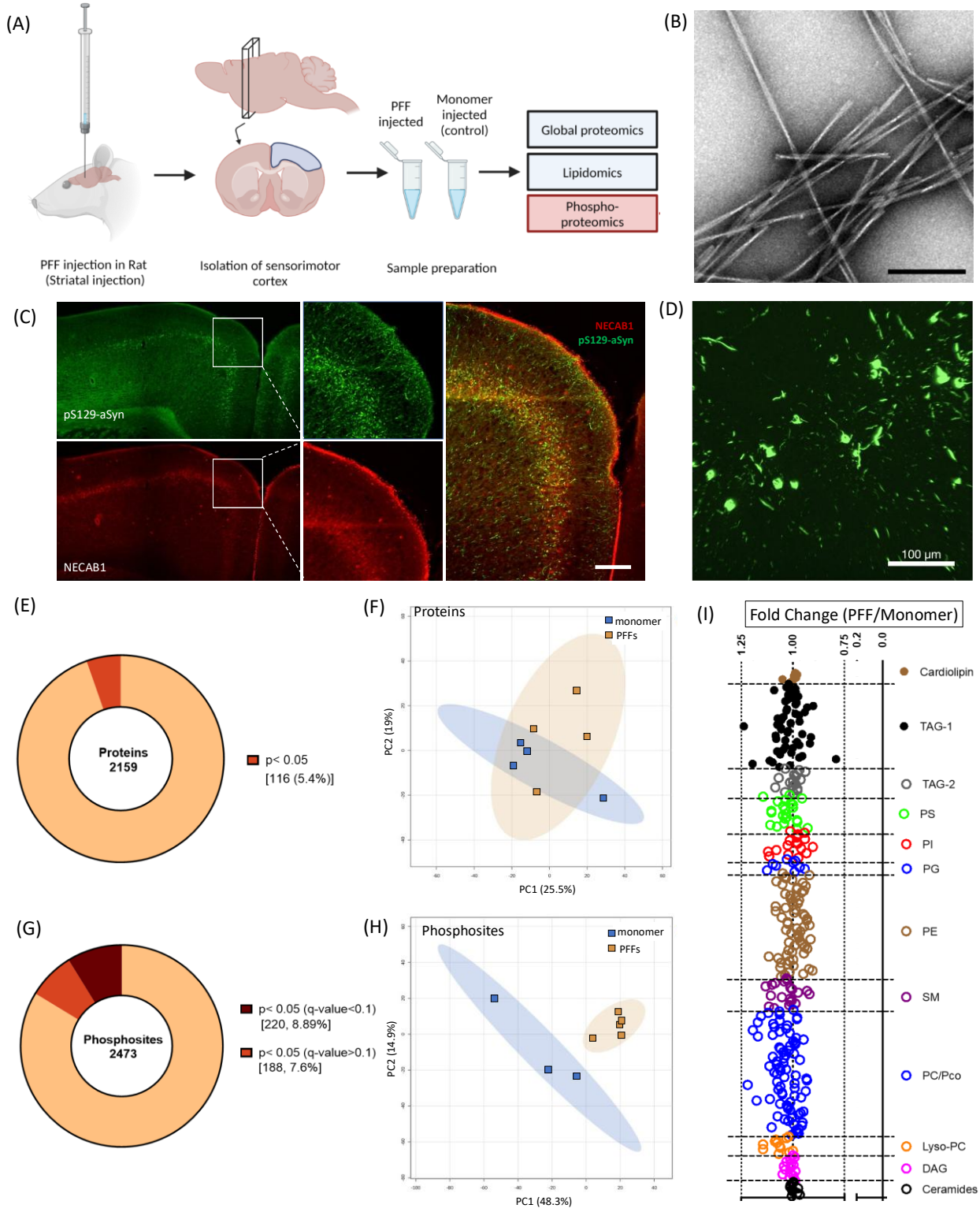
(A)
PFF injection in Rat (Striatal injection)
Isolation of sensorimotor cortex
PFF injected
Monomer injected (control)
Sample preparation
Global proteomics
Lipidomics
Phospho-proteomics
(B)
(C)
pS129-aSyn
NECAB1
NECAB1
pS129-aSyn
(D)
100 µm
(E)
Proteins 2159
p< 0.05 [116 (5.4%)]
(F)
Proteins
monomer
PFFs
PC2 (19%)
PC1 (25.5%)
(G)
Phosphosites 2473
p< 0.05 (q-value<0.1) [220, 8.89%]
p< 0.05 (q-value>0.1) [188, 7.6%]
(H)
Phosphosites
monomer
PFFs
PC2 (14.9%)
PC1 (48.3%)
(I)
Fold Change (PFF/Monomer)
1.25
1.00
0.75
0.2
0.0
Cardiolipin
TAG-1
TAG-2
PS
PI
PG
PE
SM
PC/Pco
Lyso-PC
DAG
Ceramides

**Figure 1: Rats injected intrastriatally with aSyn PFFs show evidence of phosphoproteomic changes in the sensorimotor cortex.**

(A) Overview of the multi-omics approach used to identify cortical changes associated with aSyn aggregation in the rat PFF model (created using https://BioRender.com)
(B) Representative images of aSyn preformed fibrils (PFFs) visualized by transmission electron microscopy. Scale bar: 100 nm.
(C) Representative images of a rat cortical section stained for pS129-aSyn (81a, green) and the cortical layer IV/Layer V-specific marker NECAB1 (red) 3 months after aSyn PFF injection in the striatum (n = 3 animals). Scale bar: 200 µm.
(D) Higher magnification image of the cortex from a PFF-injected rat showing pS129-aSyn aggregates resembling Lewy bodies and Lewy neurites.
(E) Pie chart representation of protein hits obtained via global proteomic analysis of homogenates prepared from rat sensorimotor cortex 3 months after intrastriatal injection with aSyn PFFs or monomer. The chart shows the percentage of hits with $p \geq 0.05$ or $p < 0.05$. Each hit was detected in ≥70% of samples in at least one experimental group.
(F) Graph showing the results of unassigned/unsupervised PCA of the $\log_2$-transformed intensities of all protein hits identified in the cortical homogenates described in (E).
(G) Pie chart representation of unique phosphosite hits obtained via phosphoproteomic analysis of the cortical homogenates described in (E). The chart shows the percentage of hits with $p < 0.05$ ($q < 0.1$) or $p < 0.05$ ($q > 0.1$). Each hit was detected in ≥70% of samples in at least one experimental group.
(H) Graph showing the results of unassigned/unsupervised PCA of the $\log_2$-transformed intensities of all phosphosite hits identified in the cortical homogenates described in (E).
(I) Graph showing lipid profiling perturbations (expressed as fold change in lipid level) in the cortical homogenates described in (E). None of the changes were below the significance threshold of $p < 0.05$. TAG, triacylglycerols; PS, phosphatidylserine; PI, phosphatidylinositol; PG, phosphatidylglycerol; PE, phosphatidylethanolamine; SM, sphingomyelin; PC, phosphatidylcholine; DAG, diacylglycerol.

## Figure 2

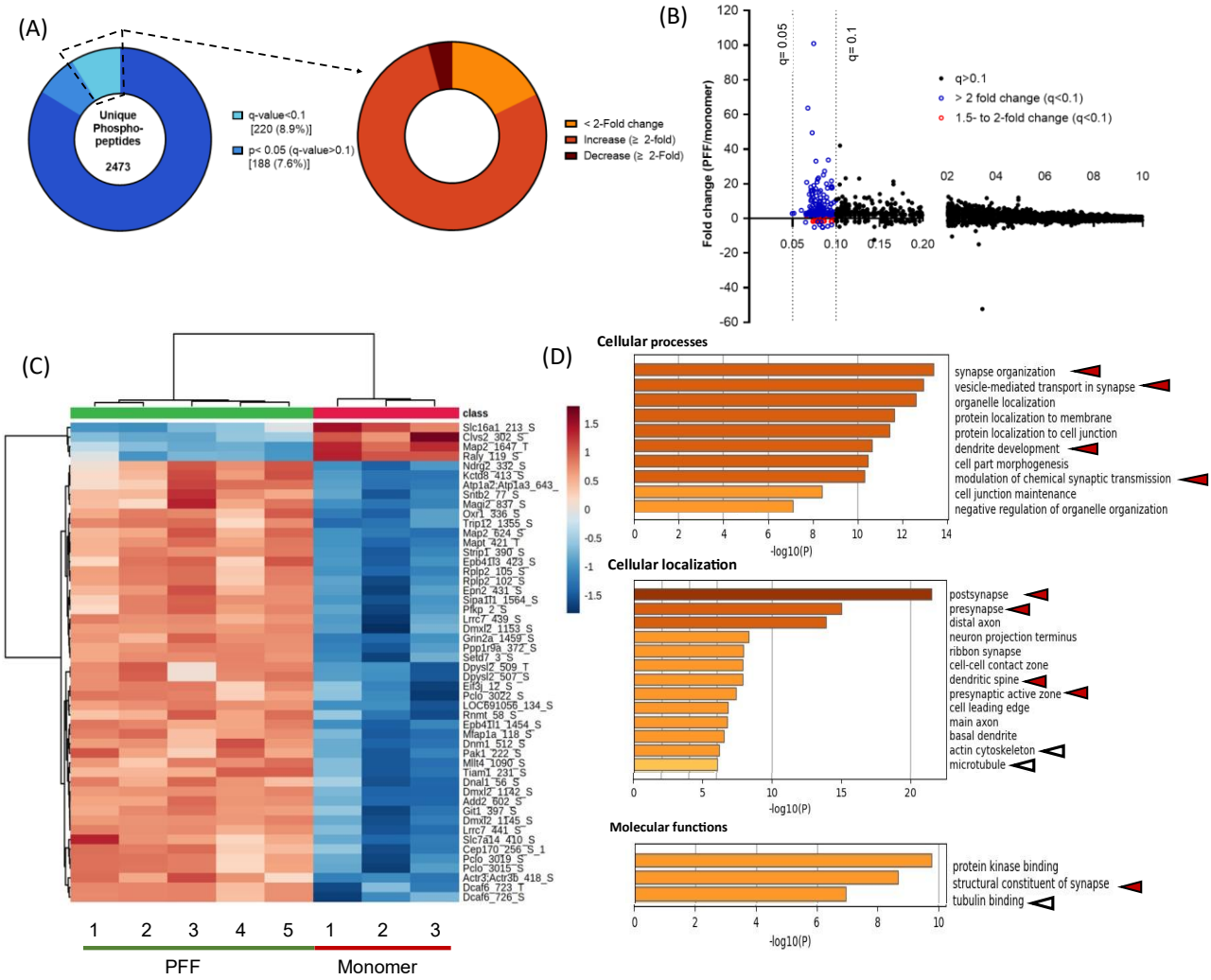
(A)
Unique Phospho-peptides
2473
q-value<0.1 [220 (8.9%)]
p< 0.05 (q-value>0.1) [188 (7.6%)]
< 2-Fold change
Increase (≥ 2-fold)
Decrease (≥ 2-Fold)
(B)
q= 0.05
q= 0.1
Fold change (PFF/monomer)
q>0.1
> 2 fold change (q<0.1)
1.5- to 2-fold change (q<0.1)
(C)
class
PFF
Monomer
(D)
Cellular processes
synapse organization
vesicle-mediated transport in synapse
organelle localization
protein localization to membrane
protein localization to cell junction
dendrite development
cell part morphogenesis
modulation of chemical synaptic transmission
cell junction maintenance
negative regulation of organelle organization
-log10(P)
Cellular localization
postsynapse
presynapse
distal axon
neuron projection terminus
ribbon synapse
cell-cell contact zone
dendritic spine
presynaptic active zone
cell leading edge
main axon
basal dendrite
actin cytoskeleton
microtubule
Molecular functions
protein kinase binding
structural constituent of synapse
tubulin binding

**Figure 2: Gene ontology analysis of the top up- or down-regulated phosphoproteins in the sensorimotor cortex of PFF-treated rats reveals perturbations of cellular structures and functions involved in synaptic transmission.**

(A) Pie chart representations of phosphosite hits obtained via phosphoproteomic analysis of homogenates prepared from rat sensorimotor cortex 3 months after intrastriatal injection with aSyn PFFs or monomer. The chart on the left is identical to that shown in Fig. 1H. The chart on the right shows the percentage of phosphosite hits with $q<0.1$ that exhibit a fold change of <2 (yellow) or are up- or down-regulated by a factor of ≥2 (orange and brown, respectively). Each hit was detected in ≥70% of samples in at least one experimental group.

(B) Plot showing the phosphosite distribution represented as intensity fold change (PFF/monomer) versus q-value. Phosphosites with $q<0.1$ that are up- or down-regulated by a factor of 1.5 to 2 or >2 are represented by red and blue symbols, respectively.

(C) Cluster heatmap showing the z-scored $\log_2$-transformed intensities of the top 50 up- or down-regulated phosphosites (i.e., phosphosites with the lowest q-values) in the cortical homogenates described in (A). Red and blue colors correspond to an increase or decrease (respectively) in phosphosite levels in rats injected with PFFs versus monomer, and the color intensity represents the Z-score-normalized $\log_2$(intensity) value. Peptide names are listed as 'protein name_phosphoresidue number'.

(D) Charts showing enriched GO terms within cellular processes (top), cellular localization (middle), and molecular functions (bottom) that represent groups of phosphoproteins in the sensorimotor cortex impacted by PFF treatment. GO analysis was carried out on proteins containing phosphosites with $q<0.1$ and a fold change of ≥2 (see panel A). Arrowheads highlight items relevant to synaptic transmission (red) or the cytoskeleton (white).

**Figure 3**

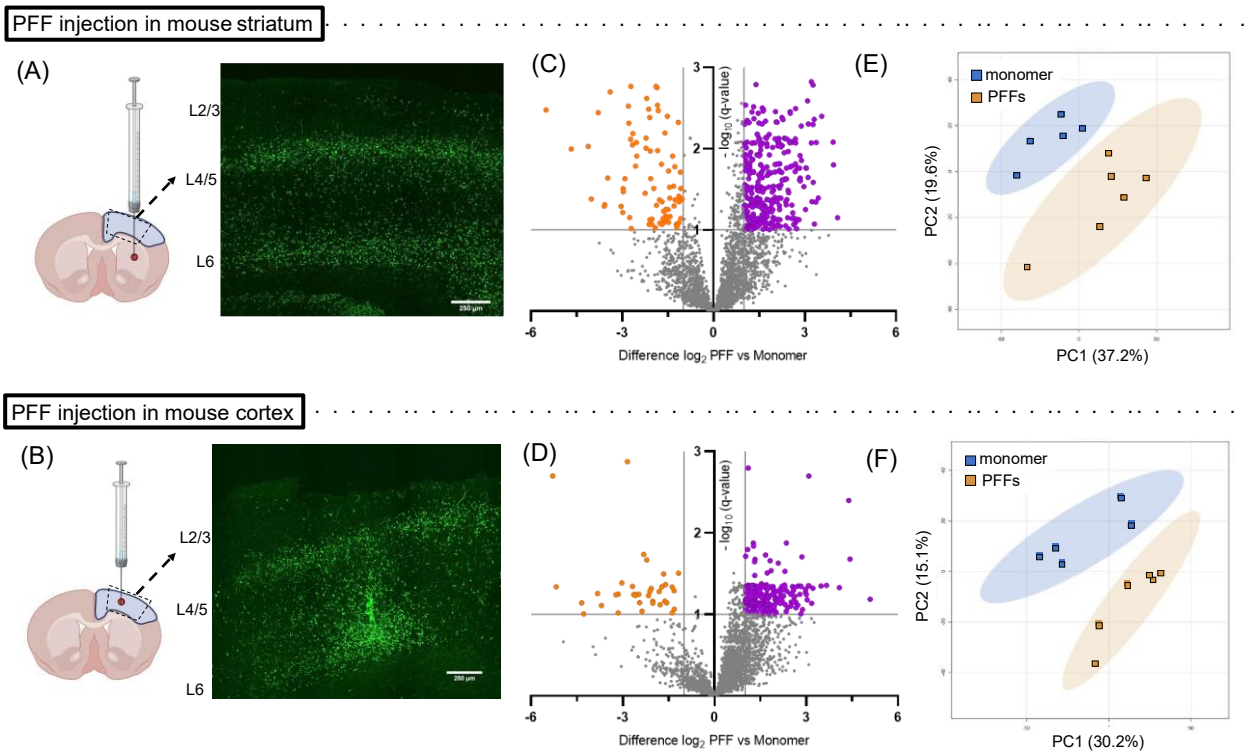


**Figure 3: Mice injected in the striatum or cortex with aSyn PFFs show evidence of phosphoproteomic changes in the sensorimotor cortex.**

(A, B) Schematics showing the injection site, tissue isolated for phosphoproteomic analysis (blue-shaded region), and approximate cortical section area processed for histology (dashed trapezoid) (LEFT), and corresponding images of pS129-aSyn immunoreactivity (EP1536Y, green) (RIGHT), for mice injected with aSyn PFFs or monomer in the striatum (A) or cortex (B). The sections were prepared 3 months after injection (scale bar: 250 µm) (n = 3 animals in each group). Schematic created using https://BioRender.com.

(C, D) Volcano plot distributions of phosphosites found to be up-regulated (purple) or down-regulated (orange) in homogenates prepared from mouse sensorimotor cortex 3 months after injection with aSyn PFFs versus monomer in the striatum (C) or cortex (D). The plot shows the fold change of the phosphosites in relation to the adjusted p-value (i.e. q-value), where $q<0.1$ was considered significant, as indicated by the horizontal dashed line.

(E, F) Graphs showing the results of unassigned/unsupervised PCA of the $\log_2$-transformed intensities of phosphosite hits in cortical homogenates from mice injected with aSyn PFFs or monomer in the striatum (E) or cortex (F), as described in (C) and (D).

## Figure 4

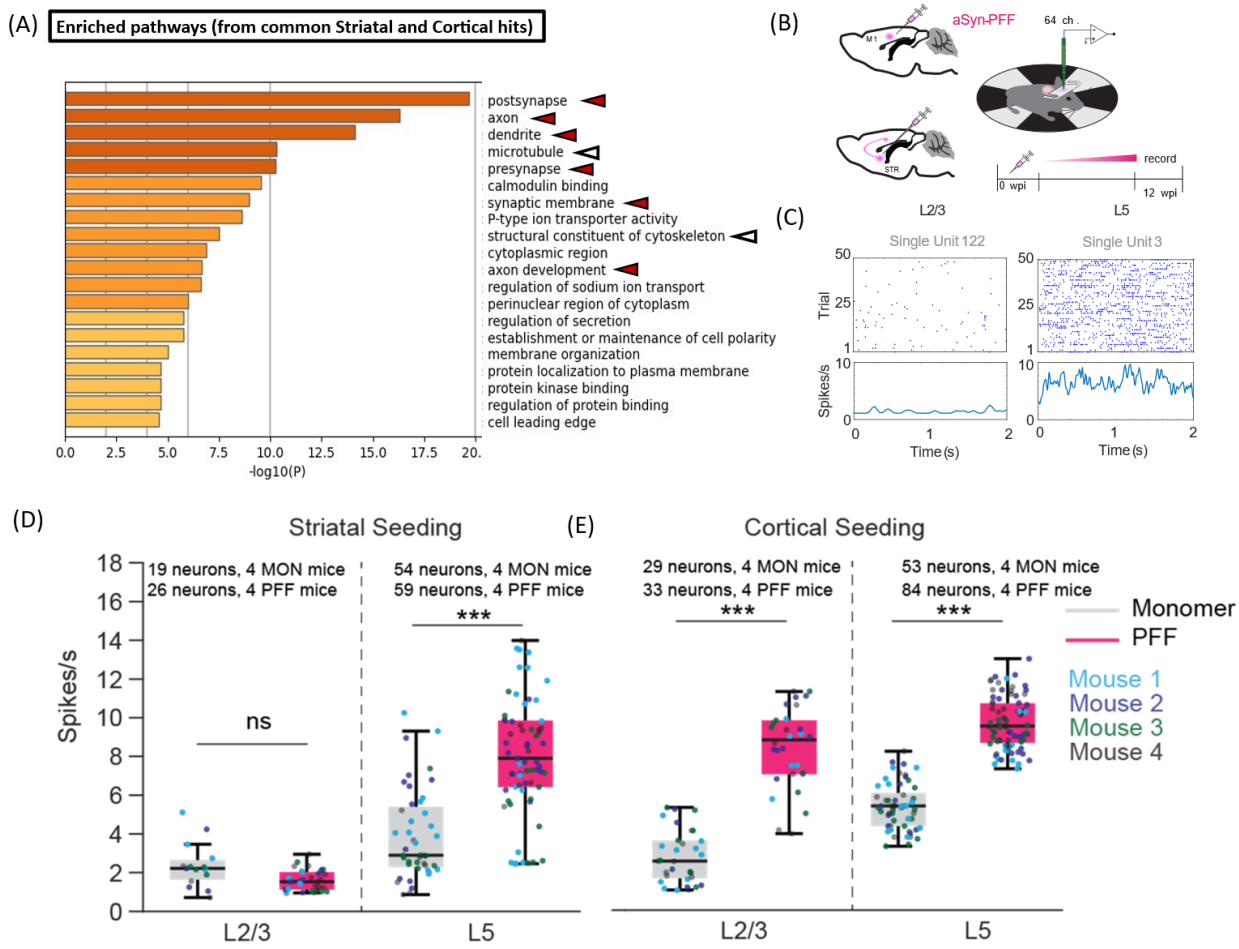
(A)
Enriched pathways (from common Striatal and Cortical hits)
postsynapse
axon
dendrite
microtubule
presynapse
calmodulin binding
synaptic membrane
P-type ion transporter activity
structural constituent of cytoskeleton
cytoplasmic region
axon development
regulation of sodium ion transport
perinuclear region of cytoplasm
regulation of secretion
establishment or maintenance of cell polarity
membrane organization
protein localization to plasma membrane
protein kinase binding
regulation of protein binding
cell leading edge
-log10(P)
(B)
aSyn-PFF
64 ch
record
0 wpi
12 wpi
L2/3
L5
(C)
Single Unit 122
Single Unit 3
Trial
Spikes/s
Time (s)
(D)
Striatal Seeding
19 neurons, 4 MON mice
26 neurons, 4 PFF mice
54 neurons, 4 MON mice
59 neurons, 4 PFF mice
ns
***
Spikes/s
L2/3
L5
(E)
Cortical Seeding
29 neurons, 4 MON mice
33 neurons, 4 PFF mice
53 neurons, 4 MON mice
84 neurons, 4 PFF mice
Monomer
PFF
Mouse 1
Mouse 2
Mouse 3
Mouse 4

**Figure 4: Mice injected with aSyn PFFs show evidence of cortical circuit dysfunction.**

(A) Chart showing enriched GO terms in the 'cellular localization' category that represent groups of phosphoproteins in mouse sensorimotor cortex impacted by PFF administration in either the striatum or cortex, 3 months after injection. GO analysis was carried out on proteins containing phosphosites with $q<0.1$ and a fold change of $\geq 2$ in at least one group (Supplementary Figure 4A,B). Arrowheads highlight items relevant to synaptic transmission (red) or the cytoskeleton (white).

(B) Schematic illustrating the design of experiments aimed at monitoring neurocircuitry function in mouse sensorimotor cortex. Two separate cohorts of mice were injected with aSyn PFFs or monomer in the primary motor cortex or dorsal striatum. Electrophysiological analyses were carried out at 0 weeks and 3 months (12 weeks) post-injection (0 and 12 wpi).

(C) Example of layer-specific unit activity during awake recording in head-fixed mice injected with aSyn monomer.

(D, E) Spiking rates of recorded neurons were analyzed based on cortical depth in mice injected with either aSyn PFFs or monomers into the striatum (D) or cortex (E). Number of neurons recorded per mouse injected in the striatum (D): L2/3 neurons, 3-6 (monomer) and 3-8 (PFF); L5 neurons, 8-15 (monomer) and 10-19 (PFF). Number of neurons recorded per mouse injected in the cortex (E): L2/3 neurons, 5-9 (monomer) and 6-8 (PFF); L5 neurons, 9-16 (monomer) and 11-30 (PFF). Each subgroup includes data from 4 animals. The box plot shows the median and interquartile range (IQR); *** $p<0.0001$, ranked-sum Wilcoxon test.

**Figure 5**

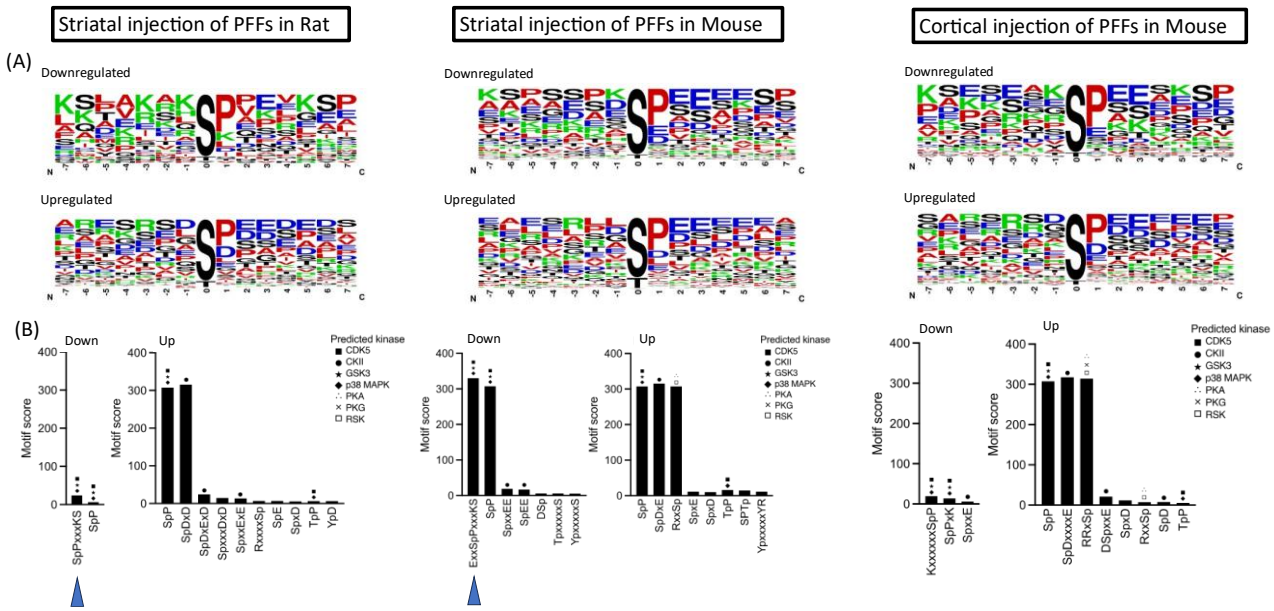


**Figure 5: Motif enrichment and kinase prediction analyses implicate altered kinase activity in aSyn PFF-induced phosphoproteomic changes.**

(A) Sequence logos illustrating the frequency of individual amino acids (with larger size indicating higher frequency) in the sequence windows of phosphosite-containing peptides that were down-regulated (top) or up-regulated (bottom) in the brains of rats injected with aSyn PFFs in the striatum (left) and mice injected with PFFs in the striatum (middle) or cortex (right). The phosphorylated residue is indicated at position 0.

(B) Bar graphs depicting enrichment scores for phosphosite motifs identified in significantly down- or up-regulated phosphosites ('down' or 'up') in the brains of rats injected with PFFs in the striatum (left) and mice injected with PFFs in the striatum (middle) or cortex (right). Higher enrichment scores indicate more significant and specific motifs. All displayed motif enrichments and kinase predictions are statistically significant ($p<1 \times 10^{-5}$ or prediction score >0.5, respectively). Symbols for predicted kinases are positioned above each bar in order of their prediction scores, with the highest score indicated by the top symbol.

**Figure 6**

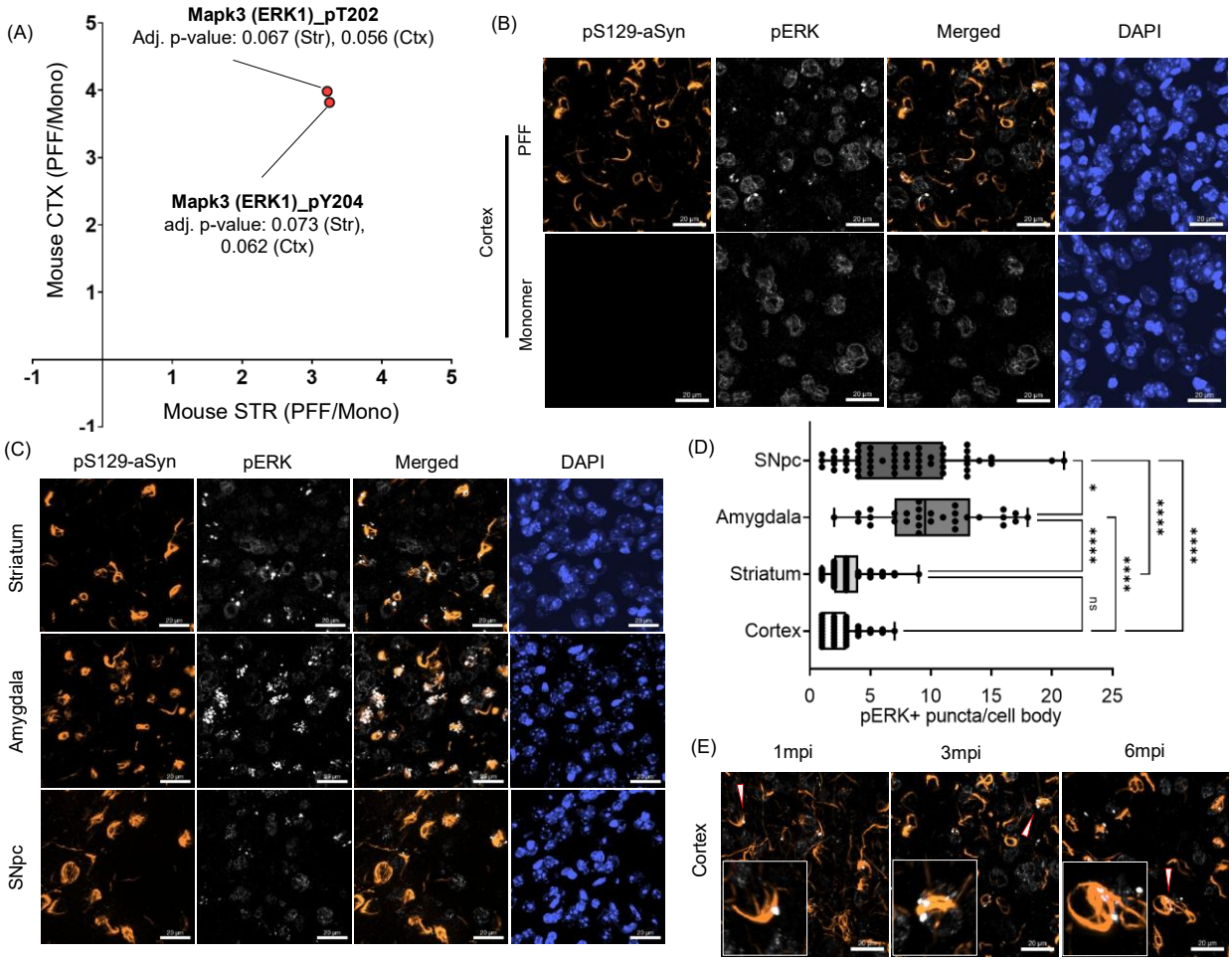


**Figure 6: The ERK pathway is activated in aSyn aggregate-containing neurons in the brains of mice injected intrastriatally with aSyn PFFs.**

A. Graph depicting the fold-change values and p-values of pT202 or pY204 in MAPK3 (ERK1)-derived peptides in the sensorimotor cortex of mice injected intrastriatally (STR) or intracortically (CTX) with aSyn PFFs versus monomer.
B. Representative images showing increased pERK puncta in aggregate-containing cortical neurons in mice injected with aSyn PFFs versus monomer (n = 4), 3 months post-injection.
C. Representative images illustrating pERK puncta in aggregate-containing neurons in the striatum, amygdala, and SNpc of mice injected with aSyn PFFs, 3 months post-injection.
D. pERK puncta counts per cell body were determined across different brain regions and are represented as box and whisker plots (n = 4 mice, > 40 total neurons per group). Statistical significance was determined using one-way ANOVA with Tukey's post hoc test (* $p < 0.05$, **** $p < 0.0001$).
E. Time-course analysis of pERK accumulation in aSyn aggregate-containing cortical neurons in PFF-injected mice at 1, 3, and 6 months post-injection (n = 3 or 4 animals/timepoint). Each inset shows a zoomed-in view of the neuron marked in the lower-magnification image by a white arrowhead.

## Supplementary Figure 1

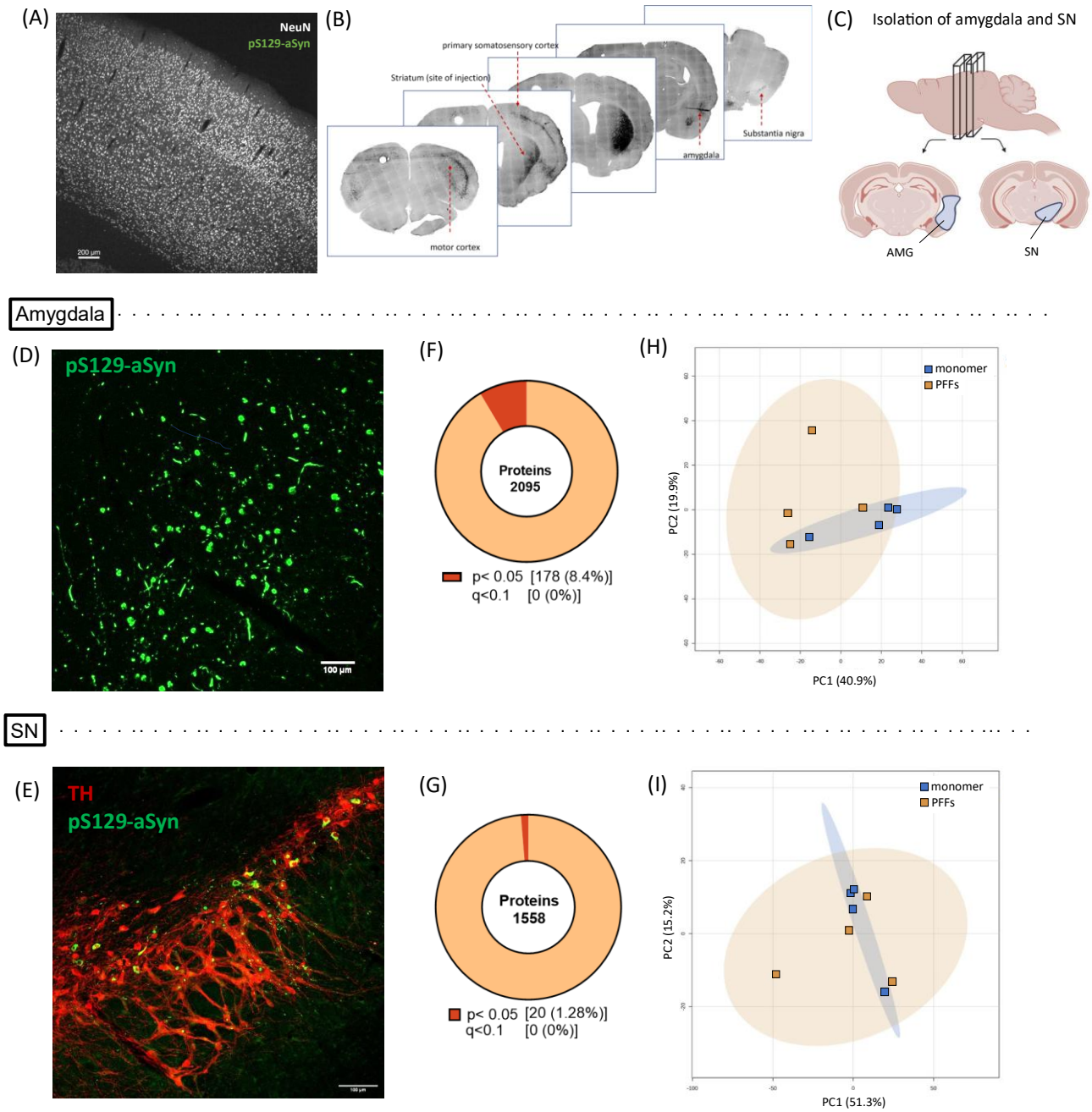

**Supplementary Figure 1: Rats injected intrastriatally with aSyn PFFs do not show evidence of pronounced changes in the global proteome in the amygdala or SN.**

(A) Image showing the absence of pS129-aSyn (81a) signal in a rat cortical section stained for the pan-neuronal marker (NeuN, white) 3 months after monomer injection in the striatum. Scale bar: 200 µm.

(B) Representative images of rat brain sections showing pS129-aSyn immunoreactivity in the cortex, striatum, amygdala, and SN 3 months after aSyn PFF injection in the striatum. Serial coronal brain sections were stained with the EP1536Y antibody.

(C) Schematic of serial brain sections used to collect amygdala (AMG) and SN samples for proteomic analysis (created using https://BioRender.com).

(D-E) Representative images of rat brain sections showing pS129-aSyn immunoreactivity (EP1536Y, green) in the amygdala (D) or SN (E) 3 months after aSyn PFF injection in the striatum. The nigral section in (E) was co-stained for tyrosine hydroxylase (TH) to demonstrate the presence of pS129-aSyn inclusions in nigral dopaminergic neurons (n = 3 animals). Scale bar: 100 µm.

(F-G) Pie chart representations of protein hits obtained via global proteomic analysis of homogenates prepared from rat amygdala (F) or SN (G) 3 months after intrastriatal injection with aSyn PFFs or monomer. The chart shows the percentage of hits with $p<0.05$ or $q<0.1$. Each hit was detected in ≥70% of samples in at least one experimental group.

(H-I) Graphs showing the results of unassigned/unsupervised PCA of the $\log_2$-transformed intensities of all protein hits identified in homogenates prepared from rat amygdala (H) or SN (I) as described in (F) and (G).

**Supplementary Figure 2**

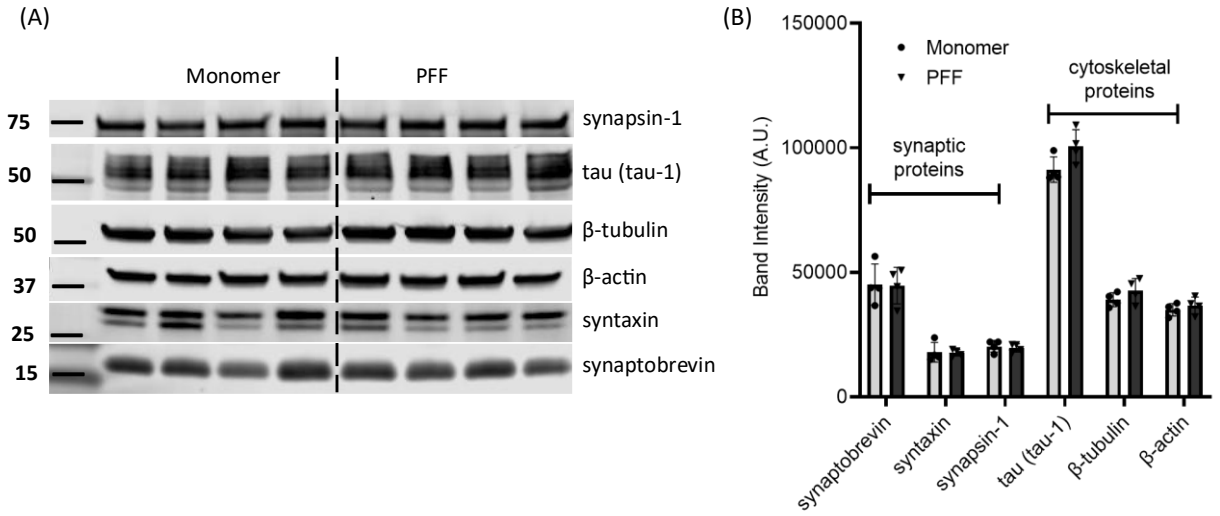


**Supplementary Figure 2: Exposure to aSyn PFFs does not lead to changes in levels of synaptic or cytoskeletal proteins in rat sensorimotor cortex.** (A) Image of Western blot loaded with homogenates prepared from rat sensorimotor cortex 3 months after intrastriatal injection with aSyn PFFs or monomer. The blot was probed with antibodies specific for the synaptic proteins synaptobrevin, syntaxin, and synapsin-1 or the cytoskeletal proteins tau, β-tubulin, and β-actin (n = 4 biological replicates). (B) Graph showing band intensities determined for the Western blot in panel A (mean ± SD). An unpaired t-test revealed no significant differences between the 'Monomer' and 'PFF' groups for each protein examined on the blot.

**Supplementary Figure 3**

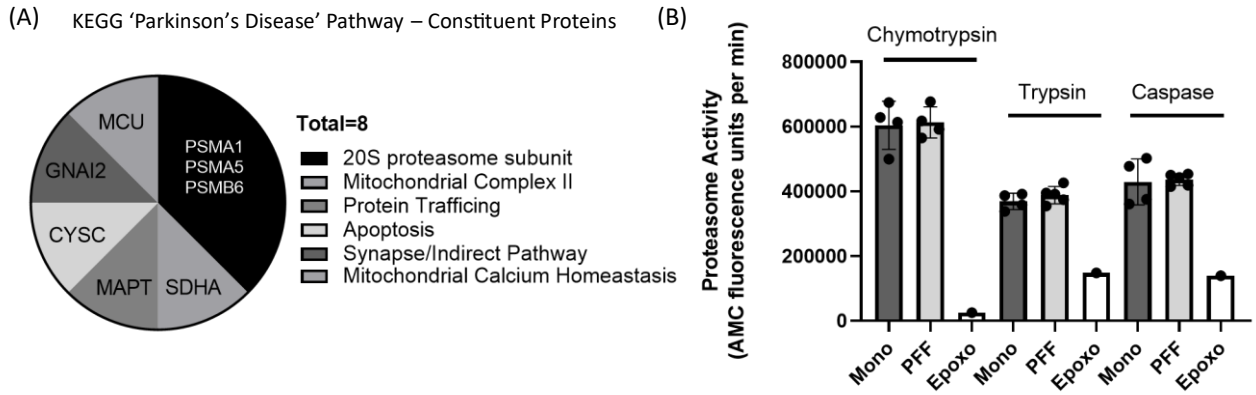


**Supplementary Figure 3: Exposure to aSyn PFFs may lead to modest changes in the levels of PD-linked proteins (including 20S proteasome subunits) in rat sensorimotor cortex.**

(A) KEGG pathway analysis of proteins from the global proteomics dataset with $p<0.05$ (Figure 1E) revealed 'Parkinson's disease' as the most significantly enriched pathway (log p = -5.17, log q = -3.21). The pie chart shows the 8 hit proteins from our dataset that constitute this pathway, classified into subgroups defined by different cellular functions. The largest subgroup ('20S proteasome subunit') contains 3 of the 8 protein hits. PSMA1, proteasome 20S subunit alpha 1; PSMA5, proteasome 20S subunit alpha 5; PSMB6, proteasome 20S subunit beta 6; SDHA, succinate dehydrogenase complex flavoprotein subunit A; MAPT, microtubule-associated protein tau; CYSC, cystatin C; GNAI2, guanine nucleotide-binding protein G(i) subunit alpha-2; MCU, mitochondrial calcium uniporter.

(B) Comparison of chymotryptic, tryptic, or caspase-like activity of the 20S proteasome in homogenates prepared from rat sensorimotor cortex 3 months after intrastriatal injection with aSyn PFFs or monomer. The graph shows enzyme activities expressed as rates of cleavage of the proteasome substrates SUC-LLVY-AMC (chymotrypsin), Boc-Leu-Arg-Arg-AMC (trypsin), and Ac-Nle-Pro-Nle-Asp-AMC (caspase-like). Bars labeled 'Epoxo' correspond to homogenates prepared from control rats, pretreated with the proteasome inhibitor epoxomicin (n = 1; final concentration, 5 μM) for 20 min prior to measuring proteasome activity (mean ± SD, n = 4 or 5 biological replicates). A one-way ANOVA revealed no significant differences between the 'Mono' and 'PFF' groups for each of the 3 enzymatic activities.

## Supplementary Figure 4

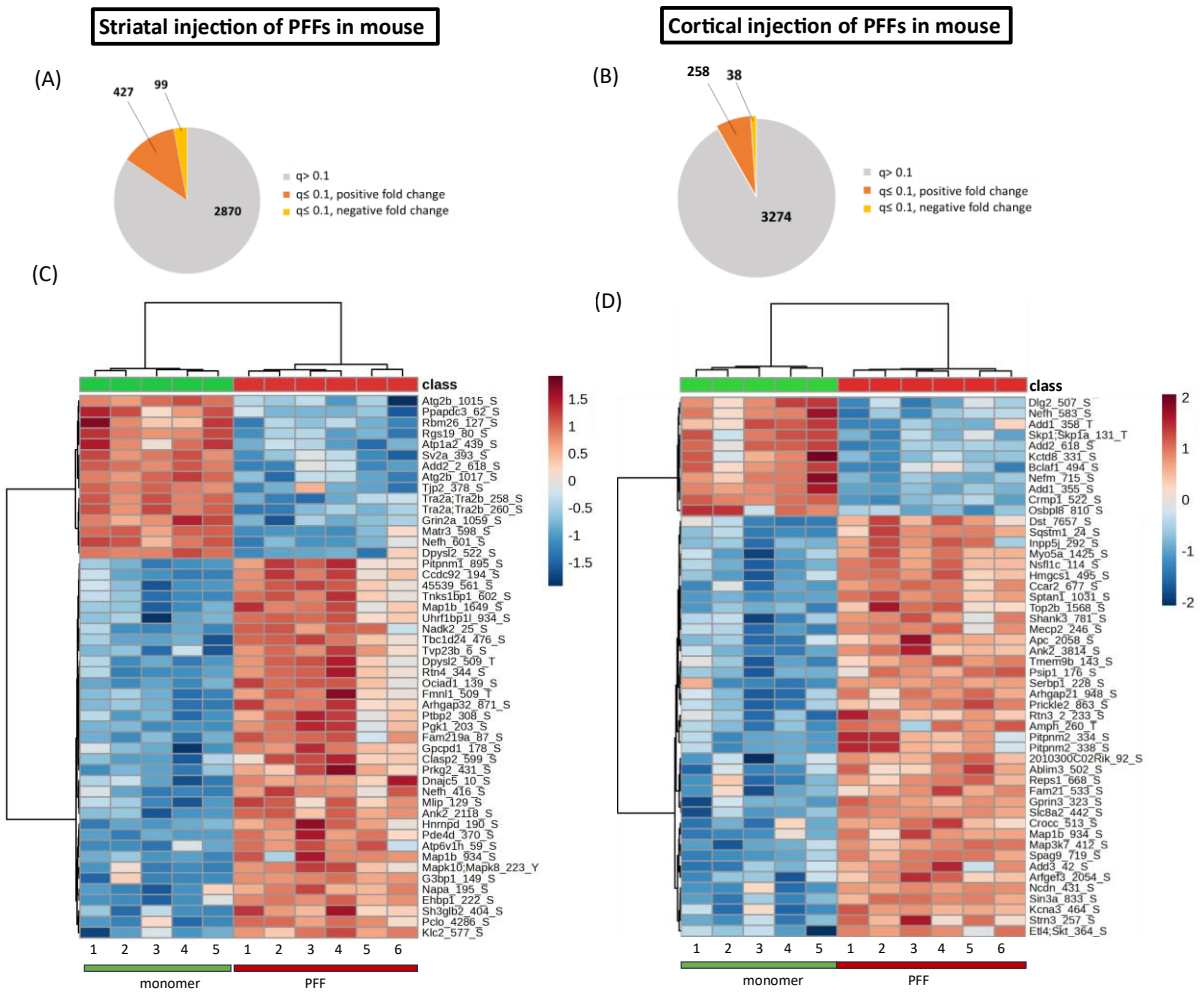


**Supplementary Figure 4: Extended analysis of phosphoproteomic changes in the sensorimotor cortex of mice following intrastriatal or intracortical injections of aSyn PFFs.**

(A, B) Pie chart representations of phosphosite hits obtained via phosphoproteomic analysis of homogenates prepared from mouse sensorimotor cortex 3 months after injection with aSyn PFFs or monomer in the striatum (A) or cortex (B). Each chart shows the percentage of hits with q<0.1 with a positive or negative fold change (orange or yellow, respectively). Each hit was detected in ≥70% of samples in at least one experimental group.

(C, D) Clustered heatmaps showing $\log_2$-transformed intensities of the top 50 up- or down-regulated phosphosites (i.e., phosphosites with the lowest q-values) in cortical homogenates from mice injected with aSyn PFFs or monomer in the striatum (C) or cortex (D), as described in (A) and (B). Red and blue colors correspond to an increase or decrease (respectively) in phosphosite levels in mice injected with PFFs versus monomer, and the color intensity represents the Z-score-normalized $\log_2$(intensity) value. Peptide names are listed as 'protein name_phosphoresidue number.'

**Supplementary Figure 5**

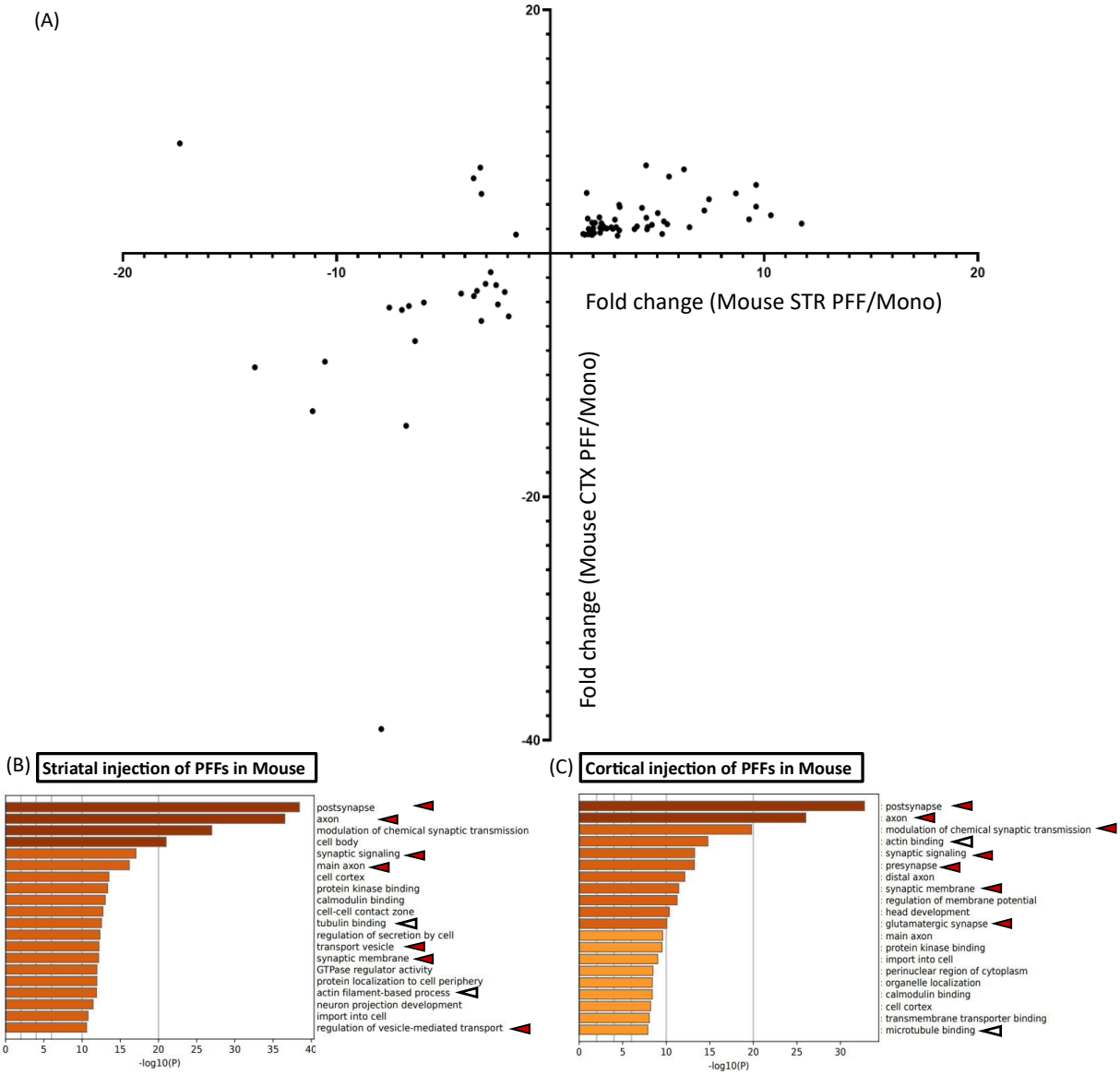


**Supplementary Figure 5: Mice injected with aSyn PFFs in the striatum or cortex show evidence of altered synaptic function and cytoskeletal organization.** (A) Graph depicting fold-change values of significantly altered phosphosites in the sensorimotor cortex of mice injected intrastriatally (STR) or intracortically (CTX) with aSyn PFFs versus monomer. (B, C) Charts showing enriched GO terms in the 'cellular localization' category that represent groups of phosphoproteins in mouse sensorimotor cortex impacted by PFF administration in the striatum (B) or cortex (C), 3 months post-injection. GO analysis was carried out on proteins containing phosphosites with q<0.1 and a fold change of ≥2 (Supplementary Figure 4A,B). Arrowheads highlight items relevant to synaptic transmission (red) or the cytoskeleton (white).

**Supplementary Figure 6**

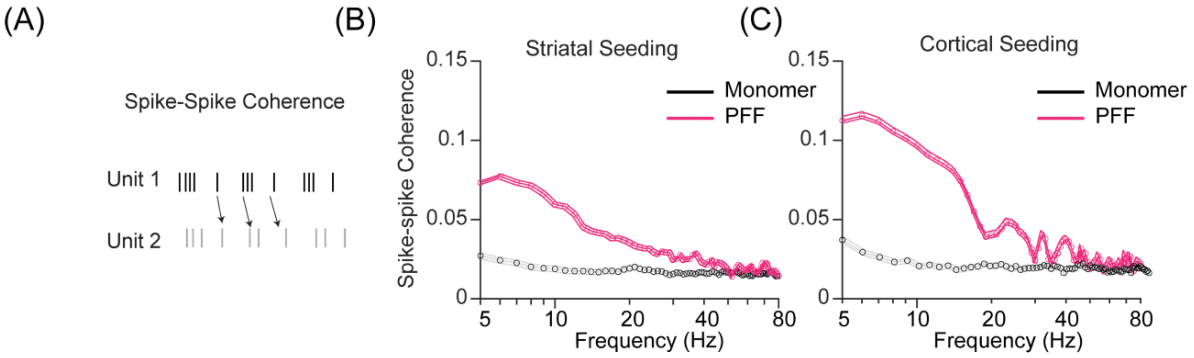


**Supplementary Figure 6: Mice injected with aSyn PFFs in the striatum or cortex show evidence of altered network connectivity.** (A) Schematic of spike-spike coherence where the coherence of two representative units is calculated based on fluctuations of spike rates (see 'Experimental Methods'). (B, C) Graphs showing frequency-resolved paired spike coherence data recorded in mouse sensorimotor cortex 3 months after injection with aSyn PFFs or monomer in the striatum (B) or cortex (C).

**Supplementary Figure 7**

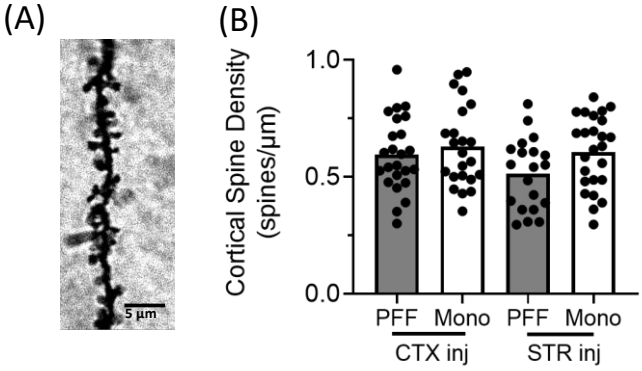


**Supplementary Figure 7: Seeded aSyn aggregation does not lead to a change in cortical spine density in our mouse PFF model.** (A) Representative image of a dendritic section from layer II/III of mouse sensorimotor cortex 3 months after intrastriatal aSyn PFF injection (scale bar: 5 µm). (B) Graph showing the spine density in sections prepared from mouse sensorimotor cortex 3 months after intracortical (CTX) or intrastriatal (STR) injection with aSyn PFFs or monomer. Five dendritic sections were analyzed per mouse, and 4 to 5 mice were analyzed per group. A one-way ANOVA revealed no significant differences among any of the groups.

**Supplementary Figure 8**

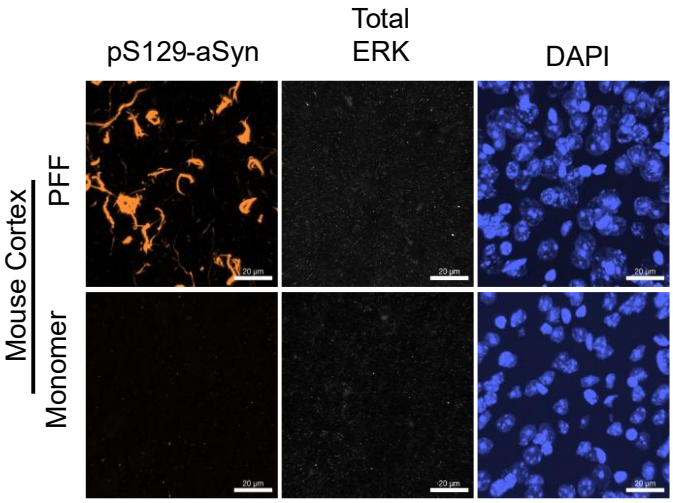


**Supplementary Figure 8: Mice show no evidence of total ERK up-regulation in aSyn aggregate-containing neurons after intrastriatal aSyn PFF injection.** Representative images show no detectable difference in total ERK levels in the sensorimotor cortex of mice injected with aSyn PFFs versus monomer 3 months post-injection (n = 4).

**Supplementary Figure 9**

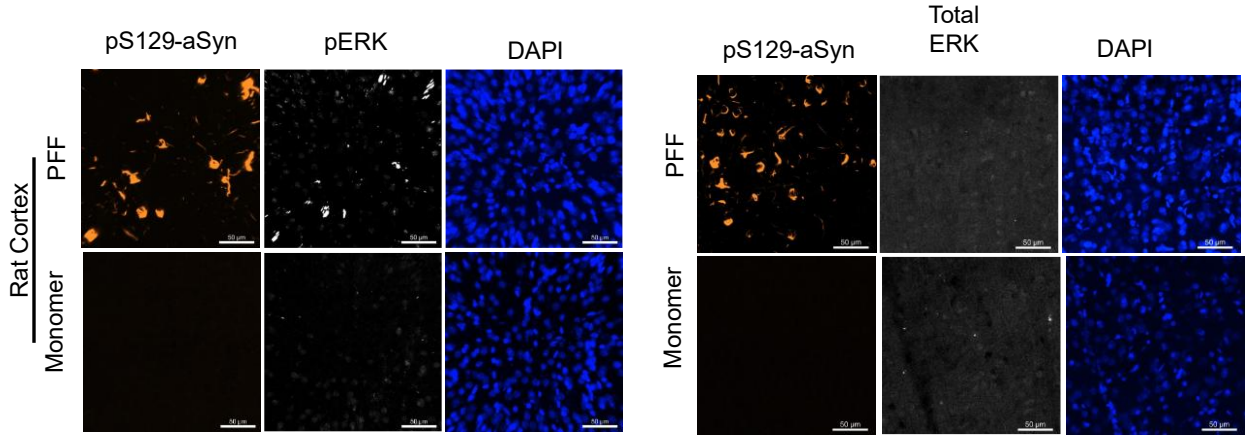


**Supplementary Figure 9: Rats injected with aSyn PFFs exhibit an increase in phospho-ERK levels.** (Left) Representative images show increased phospho-ERK (pERK) levels in the sensorimotor cortex of rats injected intrastriatally with aSyn PFFs versus monomer 3 months post-injection (n = 3), confirming ERK pathway activation. (Right) No detectable difference in total ERK levels was observed.

**Acknowledgments**

This work was supported by a Parkinson's Foundation Visiting Scholar Award, Purdue Research Foundation Grant, and Bilsland Dissertation Fellowship (to S.D.); funds from the National Institute of General Medical Sciences (T32 GM007752) through the Graduate Training Program in Cellular and Molecular Pharmacology at UCSD (to L.M.R.); National Institutes of Health grants R01AG074273 and R01AG078185 (to X. C.); and grants from the National Institutes of Health (1R21NS135424), the Clinical and Translational Sciences Institute, and Branfman Family Foundation (to J.C.R.).

**Conflict of Interest**

The authors declare no competing financial interests.

**Author contributions:**

S.D. and J.C.R. conceived the study and prepared the manuscript with input from all authors; S.D. designed and coordinated all experiments, conducted most of the experiments including PFF preparation, *in vivo* surgeries, proteomics data analysis and visualization, immunohistochemistry, and imaging; J.A.H. assisted with in vivo experiments with rats; A.N.S. and T.J. assisted with *in vivo* experiments with mice and dendritic spine analysis; A.N.S. and L.A.D. assisted with proteomics data analysis; R.M. carried out proteomics sample processing and data acquisition, and assisted with proteomics analysis; L.M.R performed motif enrichment and kinase prediction analysis; H.F.K. performed *in vivo* recording experiments; C.R.F. carried out lipid profiling sample processing and data acquisition, and assisted with lipid profiling data analysis; J.F.M. assisted with proteomics sample preparation; X.C. supervised motif enrichment and kinase prediction analysis; K.J. supervised in vivo recording experiments; U.K.A. supervised proteomics sample processing and analysis; L.V.D. supervised PFF preparation and PD modeling in rodents, provided PFF for experiments in rat, and provided input on study design; J.C.R. supervised the study.

**Data Availability**

Raw proteomics data are available. The mass spectrometry proteomics data pertaining to this study have been deposited in the ProteomeXchange Consortium via the PRIDE partner repository, with the dataset identifiers PXD057490 (rat phosphoproteome), PXD058091 (mouse phosphoproteome), and PXD057499 (rat global proteome).

## References


1. Jellinger, K.A. Dementia with Lewy bodies and Parkinson's disease-dementia: current concepts and controversies. *J Neural Transm (Vienna)* **125**, 615-650 (2018).
2. Russell, A., Drozdova, A., Wang, W. & Thomas, M. The impact of dementia development concurrent with Parkinson's disease: a new perspective. *CNS Neurol Disord Drug Targets* **13**, 1160-8 (2014).
3. Shulman, J.M., De Jager, P.L. & Feany, M.B. Parkinson's disease: genetics and pathogenesis. *Annu Rev Pathol* **6**, 193-222 (2011).
4. Crowther, R.A., Daniel, S.E. & Goedert, M. Characterisation of isolated alpha-synuclein filaments from substantia nigra of Parkinson's disease brain. *Neurosci Lett* **292**, 128-30 (2000).
5. Spillantini, M.G., Crowther, R.A., Jakes, R., Hasegawa, M. & Goedert, M. alpha-Synuclein in filamentous inclusions of Lewy bodies from Parkinson's disease and dementia with lewy bodies. *Proc Natl Acad Sci U S A* **95**, 6469-73 (1998).
6. Schweighauser, M. et al. Structures of alpha-synuclein filaments from multiple system atrophy. *Nature* **585**, 464-469 (2020).
7. Pirooznia, S.K., Rosenthal, L.S., Dawson, V.L. & Dawson, T.M. Parkinson Disease: Translating Insights from Molecular Mechanisms to Neuroprotection. *Pharmacol Rev* **73**, 33-97 (2021).
8. Braak, H. et al. Staging of brain pathology related to sporadic Parkinson's disease. *Neurobiol Aging* **24**, 197-211 (2003).
9. Beach, T.G. et al. Unified staging system for Lewy body disorders: correlation with nigrostriatal degeneration, cognitive impairment and motor dysfunction. *Acta Neuropathol* **117**, 613-34 (2009).
10. Paumier, K.L. et al. Intrastriatal injection of pre-formed mouse alpha-synuclein fibrils into rats triggers alpha-synuclein pathology and bilateral nigrostriatal degeneration. *Neurobiol Dis* **82**, 185-199 (2015).
11. Henderson, M.X. et al. Spread of alpha-synuclein pathology through the brain connectome is modulated by selective vulnerability and predicted by network analysis. *Nat Neurosci* **22**, 1248-1257 (2019).
12. Luk, K.C. et al. Pathological alpha-synuclein transmission initiates Parkinson-like neurodegeneration in nontransgenic mice. *Science* **338**, 949-53 (2012).
13. Peng, C., Trojanowski, J.Q. & Lee, V.M. Protein transmission in neurodegenerative disease. *Nat Rev Neurol* **16**, 199-212 (2020).
14. Siderowf, A. et al. Assessment of heterogeneity among participants in the Parkinson's Progression Markers Initiative cohort using alpha-synuclein seed amplification: a cross-sectional study. *Lancet Neurol* **22**, 407-417 (2023).
15. Sharma, M. & Burre, J. alpha-Synuclein in synaptic function and dysfunction. *Trends Neurosci* **46**, 153-166 (2023).
16. Runwal, G. & Edwards, R.H. The Membrane Interactions of Synuclein: Physiology and Pathology. *Annu Rev Pathol* **16**, 465-485 (2021).
17. Wang, X. et al. Pathogenic alpha-synuclein aggregates preferentially bind to mitochondria and affect cellular respiration. *Acta Neuropathol Commun* **7**, 41 (2019).
18. Zalon, A.J., Quiriconi, D.J., Pitcairn, C. & Mazzulli, J.R. alpha-Synuclein: Multiple pathogenic roles in trafficking and proteostasis pathways in Parkinson's disease. *Neuroscientist*, 10738584241232963 (2024).
19. Flores-Leon, M. & Outeiro, T.F. More than meets the eye in Parkinson's disease and other synucleinopathies: from proteinopathy to lipidopathy. *Acta Neuropathol* **146**, 369-385 (2023).

20. Fanning, S., Selkoe, D. & Dettmer, U. Vesicle trafficking and lipid metabolism in synucleinopathy. *Acta Neuropathol* **141**, 491-510 (2021).
21. Volpicelli-Daley, L.A. et al. Exogenous alpha-synuclein fibrils induce Lewy body pathology leading to synaptic dysfunction and neuron death. *Neuron* **72**, 57-71 (2011).
22. Froula, J.M. et al. alpha-Synuclein fibril-induced paradoxical structural and functional defects in hippocampal neurons. *Acta Neuropathol Commun* **6**, 35 (2018).
23. Chen, L. et al. Synaptic location is a determinant of the detrimental effects of alpha-synuclein pathology to glutamatergic transmission in the basolateral amygdala. *Elife* **11**(2022).
24. Calabresi, P., Di Lazzaro, G., Marino, G., Campanelli, F. & Ghiglieri, V. Advances in understanding the function of alpha-synuclein: implications for Parkinson's disease. *Brain* **146**, 3587-3597 (2023).
25. Calabresi, P. et al. Alpha-synuclein in Parkinson's disease and other synucleinopathies: from overt neurodegeneration back to early synaptic dysfunction. *Cell Death Dis* **14**, 176 (2023).
26. Garcia-Yague, A.J., Lastres-Becker, I., Stefanis, L., Vassilatis, D.K. & Cuadrado, A. alpha-Synuclein Induces the GSK-3-Mediated Phosphorylation and Degradation of NURR1 and Loss of Dopaminergic Hallmarks. *Mol Neurobiol* **58**, 6697-6711 (2021).
27. Ryu, M.Y. et al. Localization of CKII beta subunits in Lewy bodies of Parkinson's disease. *J Neurol Sci* **266**, 9-12 (2008).
28. Li, J. et al. Long-term potentiation modulates synaptic phosphorylation networks and reshapes the structure of the postsynaptic interactome. *Sci Signal* **9**, rs8 (2016).
29. Engholm-Keller, K. et al. The temporal profile of activity-dependent presynaptic phospho-signalling reveals long-lasting patterns of poststimulus regulation. *PLoS Biol* **17**, e3000170 (2019).
30. Kohansal-Nodehi, M., Chua, J.J., Urlaub, H., Jahn, R. & Czernik, D. Analysis of protein phosphorylation in nerve terminal reveals extensive changes in active zone proteins upon exocytosis. *Elife* **5**(2016).
31. Battis, K., Xiang, W. & Winkler, J. The Bidirectional Interplay of alpha-Synuclein with Lipids in the Central Nervous System and Its Implications for the Pathogenesis of Parkinson's Disease. *Int J Mol Sci* **24**(2023).
32. Khan, H.F. et al. Site-specific seeding of Lewy pathology induces distinct pre-motor cellular and dendritic vulnerabilities in the cortex. *Nat Commun* **15**, 10775 (2024).
33. Dent, E.W., Merriam, E.B. & Hu, X. The dynamic cytoskeleton: backbone of dendritic spine plasticity. *Curr Opin Neurobiol* **21**, 175-81 (2011).
34. Blumenstock, S. et al. Seeding and transgenic overexpression of alpha-synuclein triggers dendritic spine pathology in the neocortex. *EMBO Mol Med* **9**, 716-731 (2017).
35. Zhu, J.H., Guo, F., Shelburne, J., Watkins, S. & Chu, C.T. Localization of phosphorylated ERK/MAP kinases to mitochondria and autophagosomes in Lewy body diseases. *Brain Pathol* **13**, 473-81 (2003).
36. Hornbeck, P.V. et al. PhosphoSitePlus, 2014: mutations, PTMs and recalibrations. *Nucleic Acids Res* **43**, D512-20 (2015).
37. Tsuboi, D. et al. Dopamine drives neuronal excitability via KCNQ channel phosphorylation for reward behavior. *Cell Rep* **40**, 111309 (2022).
38. Zhang, K., Sun, L. & Kang, Y. Regulation of phosphoglycerate kinase 1 and its critical role in cancer. *Cell Commun Signal* **21**, 240 (2023).
39. Li, X. et al. Mitochondria-Translocated PGK1 Functions as a Protein Kinase to Coordinate Glycolysis and the TCA Cycle in Tumorigenesis. *Mol Cell* **61**, 705-719 (2016).
40. Kokotos, A.C. et al. Phosphoglycerate kinase is a central leverage point in Parkinson's disease-driven neuronal metabolic deficits. *Sci Adv* **10**, eadn6016 (2024).
41. Burre, J. The Synaptic Function of alpha-Synuclein. *J Parkinsons Dis* **5**, 699-713 (2015).

42. Bopp, R., Holler-Rickauer, S., Martin, K.A. & Schuhknecht, G.F. An Ultrastructural Study of the Thalamic Input to Layer 4 of Primary Motor and Primary Somatosensory Cortex in the Mouse. *J Neurosci* **37**, 2435-2448 (2017).
43. Stoyka, L.E. et al. Behavioral defects associated with amygdala and cortical dysfunction in mice with seeded alpha-synuclein inclusions. *Neurobiol Dis* **134**, 104708 (2020).
44. Goralski, T.M. et al. Spatial transcriptomics reveals molecular dysfunction associated with cortical Lewy pathology. *Nat Commun* **15**, 2642 (2024).
45. Harding, A.J. & Halliday, G.M. Cortical Lewy body pathology in the diagnosis of dementia. *Acta Neuropathol* **102**, 355-63 (2001).
46. Patterson, J.R. et al. Time course and magnitude of alpha-synuclein inclusion formation and nigrostriatal degeneration in the rat model of synucleinopathy triggered by intrastriatal alpha-synuclein preformed fibrils. *Neurobiol Dis* **130**, 104525 (2019).
47. Schulz-Schaeffer, W.J. The synaptic pathology of alpha-synuclein aggregation in dementia with Lewy bodies, Parkinson's disease and Parkinson's disease dementia. *Acta Neuropathol* **120**, 131-43 (2010).
48. Ma, S.X. et al. Complement and Coagulation Cascades are Potentially Involved in Dopaminergic Neurodegeneration in alpha-Synuclein-Based Mouse Models of Parkinson's Disease. *J Proteome Res* **20**, 3428-3443 (2021).
49. Bridi, J.C. & Hirth, F. Mechanisms of alpha-Synuclein Induced Synaptopathy in Parkinson's Disease. *Front Neurosci* **12**, 80 (2018).
50. Patterson, J.R. et al. Transcriptomic profiling of early synucleinopathy in rats induced with preformed fibrils. *NPJ Parkinsons Dis* **10**, 7 (2024).
51. Tasaki, S. et al. Inferring protein expression changes from mRNA in Alzheimer's dementia using deep neural networks. *Nat Commun* **13**, 655 (2022).
52. Mangleburg, C.G. et al. Integrated analysis of the aging brain transcriptome and proteome in tauopathy. *Mol Neurodegener* **15**, 56 (2020).
53. Parra-Rivas, L.A. et al. Serine-129 phosphorylation of alpha-synuclein is an activity-dependent trigger for physiologic protein-protein interactions and synaptic function. *Neuron* **111**, 4006-4023 e10 (2023).
54. Ramalingam, N. et al. Dynamic physiological alpha-synuclein S129 phosphorylation is driven by neuronal activity. *NPJ Parkinsons Dis* **9**, 4 (2023).
55. Ferrer, I. et al. Dysregulated protein phosphorylation: A determining condition in the continuum of brain aging and Alzheimer's disease. *Brain Pathol* **31**, e12996 (2021).
56. Okochi, M. et al. Constitutive phosphorylation of the Parkinson's disease associated alpha-synuclein. *J Biol Chem* **275**, 390-7 (2000).
57. Anderson, J.P. et al. Phosphorylation of Ser-129 is the dominant pathological modification of alpha-synuclein in familial and sporadic Lewy body disease. *J Biol Chem* **281**, 29739-52 (2006).
58. Borgo, C., D'Amore, C., Sarno, S., Salvi, M. & Ruzzene, M. Protein kinase CK2: a potential therapeutic target for diverse human diseases. *Signal Transduct Target Ther* **6**, 183 (2021).
59. Zhang, C., Vilk, G., Canton, D.A. & Litchfield, D.W. Phosphorylation regulates the stability of the regulatory CK2beta subunit. *Oncogene* **21**, 3754-64 (2002).
60. Litchfield, D.W. et al. Phosphorylation of the beta subunit of casein kinase II in human A431 cells. Identification of the autophosphorylation site and a site phosphorylated by p34cdc2. *J Biol Chem* **266**, 20380-9 (1991).
61. Rosenberger, A.F. et al. Increased occurrence of protein kinase CK2 in astrocytes in Alzheimer's disease pathology. *J Neuroinflammation* **13**, 4 (2016).
62. Fujita, K. et al. Ser46-Phosphorylated MARCKS Is a Marker of Neurite Degeneration at the Pre-aggregation Stage in PD/DLB Pathology. *eNeuro* **5**(2018).

63. Zhu, J.H., Kulich, S.M., Oury, T.D. & Chu, C.T. Cytoplasmic aggregates of phosphorylated extracellular signal-regulated protein kinases in Lewy body diseases. *Am J Pathol* **161**, 2087-98 (2002).
64. Fares, M.B., Jagannath, S. & Lashuel, H.A. Reverse engineering Lewy bodies: how far have we come and how far can we go? *Nat Rev Neurosci* **22**, 111-131 (2021).
65. Killinger, B.A. et al. In situ proximity labeling identifies Lewy pathology molecular interactions in the human brain. *Proc Natl Acad Sci U S A* **119**(2022).
66. Suzuki, H. et al. Mutant alpha-synuclein causes death of human cortical neurons via ERK1/2 and JNK activation. *Mol Brain* **17**, 14 (2024).
67. Zhang, H., Griggs, A., Rochet, J.C. & Stanciu, L.A. In vitro study of alpha-synuclein protofibrils by cryo-EM suggests a Cu(2+)-dependent aggregation pathway. *Biophys J* **104**, 2706-13 (2013).
68. Volpicelli-Daley, L.A., Luk, K.C. & Lee, V.M. Addition of exogenous alpha-synuclein preformed fibrils to primary neuronal cultures to seed recruitment of endogenous alpha-synuclein to Lewy body and Lewy neurite-like aggregates. *Nat Protoc* **9**, 2135-46 (2014).
69. Sanyal, A. et al. Alpha-Synuclein Is a Target of Fic-Mediated Adenylylation/AMPylation: Possible Implications for Parkinson's Disease. *J Mol Biol* **431**, 2266-2282 (2019).
70. Landeck, N. et al. Two C-terminal sequence variations determine differential neurotoxicity between human and mouse alpha-synuclein. *Mol Neurodegener* **15**, 49 (2020).
71. Bligh, E.G. & Dyer, W.J. A rapid method of total lipid extraction and purification. *Can J Biochem Physiol* **37**, 911-7 (1959).
72. Glatter, T. et al. Large-scale quantitative assessment of different in-solution protein digestion protocols reveals superior cleavage efficiency of tandem Lys-C/trypsin proteolysis over trypsin digestion. *J Proteome Res* **11**, 5145-56 (2012).
73. Zembroski, A.S., Buhman, K.K. & Aryal, U.K. Proteome and phosphoproteome characterization of liver in the postprandial state from diet-induced obese and lean mice. *J Proteomics* **232**, 104072 (2021).
74. Xie, Z., Ferreira, C.R., Virequ, A.A. & Cooks, R.G. Multiple reaction monitoring profiling (MRM profiling): Small molecule exploratory analysis guided by chemical functionality. *Chem Phys Lipids* **235**, 105048 (2021).
75. Reis, L.G., Casey, T.M., Sobreira, T.J.P., Cooper, B.R. & Ferreira, C.R. Step-by-Step Approach to Build Multiple Reaction Monitoring (MRM) Profiling Instrument Acquisition Methods for Class-based Lipid Exploratory Analysis by Mass Spectrometry. *J Biomol Tech* **34**(2023).
76. Tyanova, S., Temu, T. & Cox, J. The MaxQuant computational platform for mass spectrometry-based shotgun proteomics. *Nat Protoc* **11**, 2301-2319 (2016).
77. Tyanova, S. et al. The Perseus computational platform for comprehensive analysis of (prote)omics data. *Nat Methods* **13**, 731-40 (2016).
78. UniProt, C. UniProt: the universal protein knowledgebase in 2021. *Nucleic Acids Res* **49**, D480-D489 (2021).
79. Mohallem, R. & Aryal, U.K. Nuclear Phosphoproteome Reveals Prolyl Isomerase PIN1 as a Modulator of Oncogene-Induced Senescence. *Mol Cell Proteomics* **23**, 100715 (2024).
80. Zhou, Y. et al. Metascape provides a biologist-oriented resource for the analysis of systems-level datasets. *Nat Commun* **10**, 1523 (2019).
81. Pang, Z. et al. MetaboAnalyst 5.0: narrowing the gap between raw spectra and functional insights. *Nucleic Acids Res* **49**, W388-W396 (2021).
82. Berkers, C.R. et al. Profiling proteasome activity in tissue with fluorescent probes. *Mol Pharm* **4**, 739-48 (2007).
83. Ysselstein, D. et al. Effects of impaired membrane interactions on alpha-synuclein aggregation and neurotoxicity. *Neurobiol Dis* **79**, 150-63 (2015).

84. Mitra, P.P. & Pesaran, B. Analysis of dynamic brain imaging data. *Biophys J* **76**, 691-708 (1999).
85. Jarvis, M.R. & Mitra, P.P. Sampling properties of the spectrum and coherency of sequences of action potentials. *Neural Comput* **13**, 717-49 (2001).
86. Pesaran, B., Pezaris, J.S., Sahani, M., Mitra, P.P. & Andersen, R.A. Temporal structure in neuronal activity during working memory in macaque parietal cortex. *Nat Neurosci* **5**, 805-11 (2002).
87. Mitchell, C.J., De Houwer, J. & Lovibond, P.F. The propositional nature of human associative learning. *Behav Brain Sci* **32**, 183-98; discussion 198-246 (2009).
88. Crooks, G.E., Hon, G., Chandonia, J.M. & Brenner, S.E. WebLogo: a sequence logo generator. *Genome Res* **14**, 1188-90 (2004).
89. Chou, M.F. & Schwartz, D. Biological sequence motif discovery using motif-x. *Curr Protoc Bioinformatics* **Chapter 13**, 13 15 1-13 15 24 (2011).
90. Wozniak, J.M. & Gonzalez, D.J. PTMphinder: an R package for PTM site localization and motif extraction from proteomic datasets. *PeerJ* **7**, e7046 (2019).
91. Blom, N., Sicheritz-Ponten, T., Gupta, R., Gammeltoft, S. & Brunak, S. Prediction of post-translational glycosylation and phosphorylation of proteins from the amino acid sequence. *Proteomics* **4**, 1633-49 (2004).